Project number: 101111888
Project acronym: SHIMMER
Project duration: 09/2023 – 08/2026
Project Coordinator:
Andrea Alvarado Shmueli, SINTEF AS – Institute SINTEF Industry

Co-funded by the European Union

Clean Hydrogen Partnership

Horizon Europe Framework Programme (HORIZON)

HORIZON-JTI-CLEANH2-2022-05-03

Safe hydrogen injection management at network-wide level: towards European gas sector transition

Shimmer

Safe Hydrogen Injection Modelling and Management for European gas network Resilience

Deliverable 3.2. Assessing the compatibility of the existing natural gas infrastructure with H2-NG blends

VERSION	DATE	TYPE	DISSEMINATION LEVEL
03	03.08.2026	Report	PU

ABSTRACT

This deliverable presents the final outcomes of the SHIMMER structural integrity activities related to the assessment of the compatibility of existing natural gas infrastructure with hydrogen-containing gas mixtures. The work addresses two related aspects: the structural integrity and defect tolerance of repurposed pipelines under hydrogen service, and the influence of gas quality and gas composition on hydrogen embrittlement behaviour in pipeline steels.

Overall, the deliverable contributes to improving the understanding of material compatibility and integrity limitations associated with hydrogen transport in future European multi-gas networks.

AUTHORSHIP AND APPROVAL INFORMATION

AUTHOR(S) Marcos Sanchez, Nevena Marinova, Unai de Francisco Vargas, Jaime Gascon / TECNALIA	**DATE / SIGN** Day-Month-Year Marcos (Aug 26, 2026 08:29:19 GMT+2)
REVIEWED BY WP-LEADER Nevena Marinova / TECNALIA	**DATE / SIGN** Day-Month-Year Nevena Marinova Nevena Marinova (Aug 26, 2026 08:48:01 GMT+2)
APPROVED BY COORDINATOR Diana Gonzales / SINTEF	**DATE / SIGN** Day-Month-Year Diana González Diana Gonzalez (Aug 26, 2026 09:11:36 GMT+2)

Release history

VERSION	DATE	VERSION DESCRIPTION
01	03-June-2026	First version
02	23-July-2026	Revised version
03	03-August-2026	2nd revised version

The research leading to these results has received funding from Horizon Europe, the European Union's Framework Programme for Research and Innovation under grant agreement n° 101111888.

Table of contents

The research leading to these results has received funding from Horizon Europe, the European Union's Framework Programme for Research and Innovation under grant agreement n° 101111888.

Table of Figures

The research leading to these results has received funding from Horizon Europe, the European Union's Framework Programme for Research and Innovation under grant agreement n° 101111888.

List of Tables

List of Abbreviations

Term	Explanation
ANSI	American National Standards Institute
API	American Petroleum Institute
ASME	American Society of Mechanical Engineers
ASTM	ASTM International
BS	British Standard
CC220	Code Case 220
CSA	Canadian Standards Association
DMS	Dimethyl sulphide
DSO	Distribution System Operator
EM	Ethyl mercaptan
EN	European Standard
FAD	Failure Assessment Diagram
FCG	Fatigue Crack Growth
FCGR	Fatigue Crack Growth Rate
IPM	Isopropyl mercaptan
ISO	International Organization for Standardization
LNG	Liquefied Natural Gas
LVDT	Linear Variable Differential Transformer
MES	Methyl ethyl sulphide
NDT	Non-Destructive Testing
NPM	n-propyl mercaptan
RA	Reduction of Area
SEM	Scanning Electron Microscopy
SSRT	Slow Strain Rate Testing
T&D	Transmission and Distribution
TBM	tert-butyl mercaptan
TDS	Thermal Desorption Spectroscopy
THT	Tetrahydrothiophene
TSO	Transmission System Operator

The research leading to these results has received funding from Horizon Europe, the European Union's Framework Programme for Research and Innovation under grant agreement n° 101111888.

Nomenclature

Symbol / term	Description	Units / note
a	Crack depth	mm
$a0$	Initial crack depth	mm
$2c$	Surface crack length	mm
$2c0$	Initial surface crack length	mm
da/dN	Fatigue crack growth rate	mm/cycle
ΔK	Stress intensity factor range	MPa√m
K_I	Applied stress intensity factor	MPa√m
K_{mat}	Fracture toughness used in the assessment	MPa√m
K_r	Fracture ratio	Dimensionless
L_r	Load ratio	Dimensionless
$L_{r,max}$	Maximum load ratio / plastic collapse limit	Dimensionless
N	Number of fatigue cycles	cycles
OD	Pipe outside diameter	mm
OD/t	Outside diameter-to-wall-thickness ratio	Dimensionless
P	Internal pressure	bar or MPa
$P(t)$	Pressure history as a function of time	bar
t	Pipe wall thickness	mm
$\Delta\sigma$	Stress range	MPa
$\sigma(t)$	Stress history as a function of time	MPa
σ_{hoop}	Hoop / circumferential stress	MPa
σ_{ref}	Reference stress	MPa
σ_{res}	Residual stress	MPa
σ_u	Ultimate tensile strength (in the structural integrity assessment)	MPa
σ_y	Yield strength	MPa
A_i	Initial cross-sectional area	mm²
A_f	Final cross-sectional area at the necking zone	mm²
C	Compliance of the elastic region of the force-displacement curve	mm/N or equivalent
D_i	Initial specimen diameter	mm
d_1, d_2	Final neck diameters measured in two perpendicular directions	mm

The research leading to these results has received funding from Horizon Europe, the European Union's Framework Programme for Research and Innovation under grant agreement n° 101111888.

F	Applied force	N
F_{max}	Maximum load recorded during tensile testing	N
L_0	Initial gauge length	mm
ΔL	Change in length / displacement	mm
RA	Reduction of area	%
σ_{uts}	Ultimate tensile stress calculated from SSRT data	MPa
ε_{total}	Total engineering strain	% (dimensionless)
ε_{el}	Elastic strain	% (dimensionless)
ε_{pl}	Plastic strain	% (dimensionless)
H_2	Hydrogen	Gas species
H_2S	Hydrogen sulphide	Gas species
CH_4	Methane	Gas species
CO_2	Carbon dioxide	Gas species
CO	Carbon monoxide	Gas species
N_2	Nitrogen	Gas species
O_2	Oxygen	Gas species
H_2O	Water	Gas impurity
C_2H_6	Ethane	Gas species
C_2H_4	Ethylene	Gas species
SO_2	Sulphur dioxide	Gas species
COS	Carbonyl sulphide	Gas species
N_2O	Nitrous oxide	Gas species
H-gas	High-calorific natural gas blend tested in the SSRT campaign	Test environment
L-gas	Low-calorific natural gas blend tested in the SSRT campaign	Test environment
H-gas + H_2S	H-gas blend containing ppm-level H_2S and THT	Test environment

The research leading to these results has received funding from Horizon Europe, the European Union's Framework Programme for Research and Innovation under grant agreement n° 101111888.

Executive Summary

This deliverable presents the final outcomes of the structural integrity activities carried out within the SHIMMER project related to the assessment of the compatibility of existing natural gas infrastructure with hydrogen-containing gas mixtures. The work addresses two related aspects relevant to future hydrogen blending in European gas networks: (i) structural integrity and defect tolerance of repurposed pipelines, and (ii) the influence of gas composition on hydrogen embrittlement behaviour in pipeline steels.

The first part of the deliverable develops a fracture-mechanics-based assessment framework, **based on conservative assumptions**, for evaluating the suitability of existing transmission pipelines for hydrogen service. The methodology combines fatigue crack growth (FCG) analysis, fracture resistance assessment using Failure Assessment Diagrams (FAD), and defect detectability considerations. The analyses were performed using representative pipeline geometries, operational conditions, and material grades relevant to the European transmission network. The results show that hydrogen exposure significantly accelerates fatigue crack growth and reduces fracture resistance, particularly at high operating pressures and for pipelines with high diameter-to-thickness ratios. The study also highlights that hydrogen can reduce the margin between detectable and critical defects, demonstrating the importance of considering inspection capability together with structural integrity assessment when evaluating hydrogen repurposing scenarios.

Overall, the assessment provides a structured basis for ranking repurposing scenarios and identifying where additional integrity work is required. It does not establish universal hydrogen blending limits or provide final acceptance decisions for individual pipelines. A favourable screening result indicates a lower relative concern under the adopted assumptions, whereas an unfavourable result identifies the need for additional evidence or mitigation before hydrogen-containing service is considered.

The second part investigates the influence of representative European gas compositions on hydrogen embrittlement behaviour in API 5L X70 pipeline steel under high-pressure gaseous environments. Slow strain rate testing (SSRT) and post-mortem fracture analysis were performed using gas mixtures representative of H-gas and L-gas compositions currently present or expected in the European gas transmission grid, including blends containing H_2S and sulphur containing odorant. Differences between gas compositions were observed, although the results suggest that hydrogen-assisted degradation in complex gas mixtures cannot be directly attributed to a single gaseous component or simple cumulative effects.

About the project: The European natural gas infrastructure provides the opportunity to accept hydrogen (H_2), as a measure to integrate low-carbon gases while leveraging the existing gas network and contributing to decarbonisation. However, there are technical and regulatory gaps that should be closed, adaptations and investments to be made to ensure that multi-gas networks across Europe will be able to operate in a reliable and safe way while providing a highly controllable gas quality and required energy demand. Aspects such as material integrity of pipelines and components, as well as the lack of harmonisation of gas quality requirements at European level must be addressed in order to facilitate the injection of H_2 in the natural gas network.

In this context, the SHIMMER project (Safe Hydrogen Injection Modelling and Management for European gas network Resilience) was selected for funding as part of the 2023 Clean Hydrogen Partnership programme. SHIMMER aims to enable a higher integration of low-carbon gases and safer H_2 injection management in multi-gas networks by strengthening the knowledge base and improving the understanding of risks and opportunities in H_2 projects.

It will do this by:

- Mapping and assessing European gas T&D infrastructure in relation to materials, components, technology, and their readiness for hydrogen blends.
- Defining methods, tools and technologies for multi-gas network management and quality tracking, including simulation, prediction, and safe management of network operation in view of widespread hydrogen injection in a European-wide context.

The research leading to these results has received funding from Horizon Europe, the European Union's Framework Programme for Research and Innovation under grant agreement n° 101111888.

- Proposing best practice guidelines for handling the safety of hydrogen in the natural gas infrastructure and managing the risks.

1 Introduction

1.1 Purpose of the document

This deliverable represents the final outcome of the research activities carried out within the task focused on the evaluation of materials and components qualification procedures for assessing hydrogen readiness, as part of the **Integrity Management and Safety Work Package 3** developed within the SHIMMER project. The deliverable addresses the compatibility of existing natural gas infrastructure with hydrogen-containing gas mixtures through two distinct but related aspects. The first part of the deliverable focuses on the structural integrity assessment and defect tolerance of existing transmission pipelines under hydrogen service. A fracture-mechanics-based framework combining fatigue crack growth, fracture resistance, and defect detectability is developed to assess the suitability of repurposed pipelines operating under hydrogen-containing conditions.

The second part investigates the influence of gas quality and gas composition on hydrogen embrittlement behaviour in pipeline steels under representative gaseous environments. Particular attention is given to the role of natural gas constituents, impurities, and sulphur-containing species on hydrogen-assisted degradation mechanisms. The investigated gas mixtures were selected to reflect representative compositions currently present or expected in the European gas transmission grid, ensuring that the experimental conditions remain as close as possible to realistic future operating scenarios for hydrogen–natural gas transport systems.

Together, these studies contribute to improving the understanding of how both structural integrity limitations and gas composition effects influence the compatibility of existing gas infrastructure with hydrogen transport. The deliverable therefore contributes to the development of safe and reliable hydrogen repurposing and integrity-management strategies for future European multi-gas networks.

1.2 Authorship and Intellectual Property Rights

The preparation of this report was led by Tecnalia, who were responsible for compiling and structuring the findings. Following its preparation, the report was circulated to all consortium members for review and revision, ensuring that the perspectives, expertise, and feedback of the entire partnership were incorporated.

1.3 Intended readership

This deliverable is intended for technical experts, researchers, gas transmission and distribution operators (TSOs and DSOs), infrastructure owners, engineering companies, integrity-management specialists, standardization bodies, and regulatory stakeholders involved in the assessment of hydrogen transport in existing natural gas infrastructure.

The work combines fracture-mechanics-based structural integrity assessment with experimental investigation of hydrogen embrittlement under representative gas compositions relevant to the European gas transmission grid. The presented methodologies, the use of industrially relevant datasets, and experimental results contribute to improving the understanding of hydrogen-related degradation mechanisms, defect tolerance, and gas composition effects in hydrogen-containing transmission systems. The findings are therefore relevant for both research activities and future technical assessment methodologies related to hydrogen repurposing and integrity management of European multi-gas networks.

1.4 Structure of this document

This deliverable is divided into two main parts. The first part focuses on the structural integrity assessment and defect tolerance of existing natural gas pipelines under future hydrogen blending scenarios. The second part investigates the influence of gas quality and gas composition on hydrogen embrittlement behaviour in pipeline steels under representative gaseous environments.

The research leading to these results has received funding from Horizon Europe, the European Union's Framework Programme for Research and Innovation under grant agreement n° 101111888.

1.5 Stakeholder involvement

The work was developed in close collaboration with the industrial partners participating in the SHIMMER consortium, including TSOs and DSOs together with their technical teams. Their input contributed to the definition of representative operating conditions, gas compositions, and integrity assessment scenarios relevant to the European gas transmission network. In particular, the industrial partners provided operationally relevant data related to pipeline materials, geometries, and operating conditions, and supported the definition of representative gas compositions for hydrogen transport applications.

1.6 Relation to other projects and initiatives

Some of the conclusions related to the assessment of gas composition presented build upon previous research activities related to hydrogen embrittlement in pipeline steels. In particular, interpretation of the results related to sulphur-containing odorants was supported by previous findings obtained within the ONTZHi project, coordinated by Tecnalia, where commercially relevant THT concentrations showed no significant enhancement of hydrogen-assisted degradation under high-pressure gaseous hydrogen conditions. However, this interpretation is made with caution, since the effect of gas additives may differ in complex multicomponent gas mixtures.

1.7 Relationship with other deliverables

The work presented in this document receives inputs from the following deliverables:

- D2.4 Scope and limitations of standards for testing and qualifications of materials and components for H2 service
- D3.1 Identification of critical material properties and component factors

The research leading to these results has received funding from Horizon Europe, the European Union's Framework Programme for Research and Innovation under grant agreement n° 101111888.

2 Structural integrity screening of repurposed natural gas pipelines

2.1 Objectives and scope of the assessment

The transition towards low-carbon energy systems has increased the interest in hydrogen as an energy carrier capable of supporting decarbonisation across multiple industrial sectors. In this context, repurposing existing natural gas transmission pipelines for hydrogen transport has emerged as a cost-effective and scalable strategy compared to building dedicated hydrogen pipelines from scratch [1,2].

However, the introduction of hydrogen into steel pipelines, either as a pure gas or as a blend with natural gas, raises structural integrity challenges. A key issue is whether defects that are acceptable under natural gas service remain tolerable under hydrogen exposure. From a structural integrity perspective, this question is critical because crack-like defects may propagate under cyclic internal pressure and eventually reach a critical fracture condition.

Extensive literature has demonstrated that hydrogen affects the mechanical behaviour of steels in ways that are directly relevant to defect tolerance. In particular, hydrogen exposure can reduce fracture toughness and accelerate fatigue crack growth (FCG) [3–8]. These effects are commonly interpreted in terms of hydrogen-assisted damage mechanisms, including hydrogen-enhanced localized plasticity and hydrogen-enhanced decohesion, together with hydrogen diffusion and trapping processes that modify crack-tip conditions and facilitate crack advance under monotonic and cyclic loading [9–11].

Recent studies have assessed the structural integrity of repurposed pipelines for the introduction of hydrogen blends. They argued that the main integrity consequences arise from the combination of lower fracture toughness and accelerated FCG, all of which reduce the tolerance to defects in service [12]. In parallel, emerging fracture-assessment approaches have shown that conventional Failure Assessment Diagram (FAD) methodologies can be extended to hydrogen transmission scenarios, including weld-sensitive and hydrogen-dependent conditions, but they also show that the outcome is highly sensitive to the representation of residual stresses, local brittle regions, and degraded material properties [13]. Recent work on ASME B31.12 Option A has also shown that current code-based repurposing assessments may contain significant conservatism, supporting the need for more explicit and mechanically grounded evaluations rather than relying on blanket assumptions [14]. At the same time, recent reviews of standards and codes have concluded that important gaps remain in test methods, material qualification routes, and integrity-assessment procedures for hydrogen pipeline infrastructure [15].

Within this context, the present section reports the structural integrity screening activity performed in SHIMMER to evaluate representative natural gas pipeline repurposing scenarios under hydrogen-containing service. The assessment combines fracture-mechanics-based critical defect evaluation with fatigue crack growth calculations under representative operational pressure fluctuations. Hydrogen effects are introduced through degraded fracture toughness values compiled from the literature and through hydrogen-adjusted FCG laws. Defect detectability is also considered at screening level by comparing representative detectable flaw sizes with calculated critical defect conditions.

The objective of this section is to provide an assessment of the influence of material grade, pipeline geometry, operating pressure and hydrogen fraction on fatigue life and defect tolerance. The results are intended to support the identification of configurations that may remain within conservative screening margins and those for which a more detailed, case-specific structural integrity assessment would be required before hydrogen service.

2.2 Engineering basis and assessment assumptions

The structural integrity screening performed in this section is based on recognised fracture-mechanics and fatigue-assessment procedures, combined with conservative assumptions suitable for a project-level evaluation of hydrogen repurposing scenarios. The assessment focuses on crack-like defects in transmission pipelines, since these defects are directly relevant to both fracture resistance and fatigue crack growth under cyclic internal pressure.

The research leading to these results has received funding from Horizon Europe, the European Union's Framework Programme for Research and Innovation under grant agreement n° 101111888.

The engineering basis of the assessment combines three complementary elements. First, a fracture assessment procedure is used to determine critical defect conditions for representative pipeline geometries and material grades. Second, fatigue crack growth calculations are performed to estimate the evolution of detectable crack-like defects under operational pressure fluctuations. Third, defect detectability is considered by comparing representative detectable flaw dimensions with the calculated critical defect conditions. This combination allows the screening to evaluate not only whether a defect may become critical, but also whether sufficient margin exists between detection and failure.

The assessment follows a conservative screening philosophy. Hydrogen effects are introduced through two main material-degradation aspects: reduction of fracture toughness and acceleration of fatigue crack growth. These effects are represented using literature-based material data and hydrogen fatigue crack growth laws available in recognised engineering guidance. Where uncertainty exists, conservative assumptions are adopted in order to avoid overestimating the integrity margin of existing pipelines.

The fracture assessment is based on the Failure Assessment Diagram (FAD) approach, following the general principles of BS 7910. The analysis considers semi-elliptical internal axial surface flaws in cylindrical pipelines subjected to internal pressure. This flaw configuration is relevant for transmission pipelines because internal pressure primarily generates circumferential stresses, which drive axial crack opening. The assessment is performed using an Option 1 screening approach and simplified loading assumptions, with membrane stress from internal pressure as the main primary stress contribution.

Fatigue crack growth is assessed from an initial detectable defect size to the critical defect condition obtained from the fracture assessment. The cyclic loading input is derived from representative operational pressure fluctuations. Since long-term hydrogen transmission pressure records are still limited, natural gas pressure histories are used as baseline operational loading spectra, while hydrogen effects are introduced through material behaviour. The pressure signal is converted into hoop stress history and processed using rainflow cycle counting to obtain a stress-range spectrum suitable for fatigue crack growth calculations.

The case matrix includes representative API pipeline steel grades, medium and large pipeline geometries, operating pressures, and hydrogen fractions in the transported gas. Material strength properties are defined according to minimum requirements from applicable pipeline guidance, while fracture toughness and fatigue crack growth behaviour are selected to provide conservative screening conditions. The initial defect size is defined using representative non-destructive testing detectability thresholds, allowing the assessment to estimate the remaining margin between a detectable flaw and the critical condition.

Overall, the assumptions adopted in this section are intended to support a conservative comparison between different repurposing scenarios rather than to define absolute acceptance limits for individual pipelines. Pipeline-specific assessments would require more detailed information on material properties, weld condition, residual stresses, defect morphology, inspection performance, pressure history and applicable safety factors.

2.2.1 Structural integrity assessment approach

The structural integrity assessment was performed using a fracture-mechanics-based screening approach consistent with the general principles of BS 7910. The objective was to determine whether representative crack-like defects in existing natural gas pipelines may remain acceptable under hydrogen-containing service, considering both fracture resistance and plastic collapse.

The assessment was based on the FAD concept, which evaluates the condition of a flawed component through two non-dimensional parameters: the fracture ratio, K_r, and the load ratio, L_r. The fracture ratio represents the applied crack-driving force normalised by the material fracture resistance, while the load ratio represents the proximity of the component to plastic collapse. A defect is considered acceptable when the corresponding assessment point remains within the safe region of the FAD.

The fracture ratio was defined as:

$$\boldsymbol{K_r = \frac{K_I}{K_{mat}}} \qquad \text{Equation 1}$$

The research leading to these results has received funding from Horizon Europe, the European Union's Framework Programme for Research and Innovation under grant agreement n° 101111888.

where K_I is the applied stress intensity factor and K_{mat} is the fracture toughness used in the assessment. The load ratio was defined as:

$$L_r = \frac{\sigma_{ref}}{\sigma_y} \quad \text{Equation 2}$$

where σ_{ref} is the reference stress and σ_y is the material yield strength.

Figure 1 schematically illustrates the FAD concept. The failure assessment line separates acceptable and unacceptable conditions. Assessment points located below the line are considered safe, while points located on the line correspond to critical conditions. Points above the line are considered unsafe. The diagram also illustrates the transition between brittle fracture-dominated behaviour, elastoplastic fracture behaviour and plastic collapse-dominated behaviour as (L_r) increases.

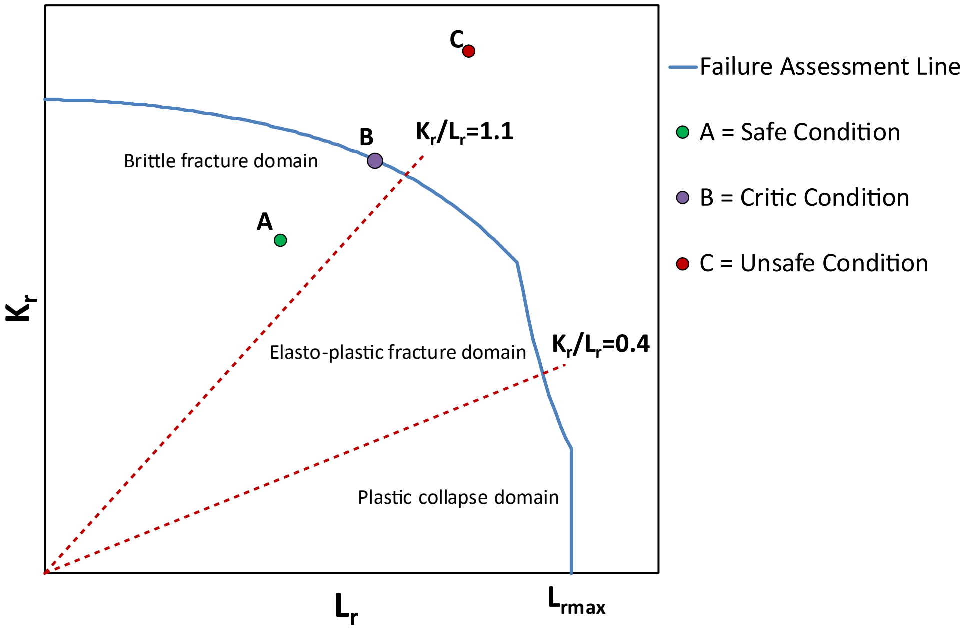

Figure 1 Failure assessment diagram (FAD) definition.

The analysis focused on semi-elliptical internal axial surface flaws in cylindrical pipelines subjected to internal pressure. This flaw configuration was selected because internal pressure mainly generates circumferential stress, which is the primary driving stress for axial crack opening. The circumferential stress was evaluated using the thin-wall Barlow expression:

$$\sigma_{hoop} = \frac{P \cdot OD}{2t} \quad \text{Equation 3}$$

where (P) is the internal pressure, (OD) is the outer diameter and (t) is the pipe wall thickness.

The applied stress intensity factor was calculated using the corresponding BS 7910 solutions for semi-elliptical internal axial surface cracks for pipelines. Stress concentration and misalignment factors were taken as unity. Residual stresses were treated as secondary stresses and an initial as-welded residual stress equal to the material yield strength was assumed. Within the FAD calculation, the effective residual stress contribution was limited according to the interaction between primary loading, flow stress and secondary stress prescribed by the adopted BS 7910 procedure.

For each material, geometry and pressure condition, the critical defect size was obtained by increasing the crack dimensions until the FAD assessment reached the limiting condition. Since a semi-elliptical surface flaw is defined by both crack depth, a, and surface length, 2c, the result of the assessment is not a single critical crack size but a critical defect envelope in the a-2c space.

The research leading to these results has received funding from Horizon Europe, the European Union's Framework Programme for Research and Innovation under grant agreement n° 101111888.

The calculated critical defect envelopes were subsequently compared with representative non-destructive testing detectability thresholds. This comparison provides a screening-level indication of whether defects that are large enough to be detected by inspection still retain sufficient margin before reaching critical conditions.

The approach was intended to provide conservative trends across representative repurposing scenarios rather than pipeline-specific acceptance decisions. More detailed assessments would require project-specific information on actual material toughness, weld condition, residual stress state, flaw morphology, inspection performance and operating history.

2.2.2 Fatigue crack growth assessment

The fatigue crack growth assessment was performed to estimate the evolution of representative crack-like defects under cyclic internal pressure. The analysis considered the propagation of an initial detectable flaw up to the critical defect condition obtained from the fracture assessment described in Section 2.2.1.

Crack propagation was modelled using a fracture-mechanics-based approach, where the crack growth rate is expressed as a function of the stress intensity factor range: $da/dN = f(\Delta K)$.

The initial crack dimensions were set to a_0=2 mm and $2c_0$=20 mm as study-specific, technique-independent reference dimensions selected with reference to the indicative inspection capabilities reported in Annex T of BS 7910. This ensures that the fatigue-life calculation represents the remaining life of a defect from the point at which it is assumed to be detectable by non-destructive testing, rather than the total life from crack initiation. In the screening assessment, the final crack size was defined as the critical defect condition obtained from the FAD-based assessment.

The reference crack dimensions adopted in this study should be understood as study-specific screening assumptions. To set the initial crack defect dimensions there are further, less conservative options (see DVGW G464 [16]), allowing to define a smaller defect size dimension. Furthermore, the SHIMMER consortium is aware of other relevant standards that are currently under revision with this area as well.[17]

Figure 2 schematically illustrates the two mechanisms through which hydrogen is considered in the overall assessment: acceleration of fatigue crack growth and reduction of fracture toughness. These mechanisms are evaluated separately in the present screening framework. In the fatigue-life calculations, a common conservative value of K_{mat} =55 MPa√m was used for all environments, and the hydrogen fraction therefore affects fatigue life through the adopted hydrogen-assisted fatigue crack growth law.

In order to maintain a conservative screening approach, hydrogen-assisted fatigue crack growth was represented using the ASME B31.12 Code Case 220 formulation [18]. This approach accounts for the influence of hydrogen pressure and load ratio through a conservative fatigue crack growth envelope, making it suitable for project-level screening where material-specific fatigue crack growth data are not available for every steel grade and condition.

For each case, the crack was incrementally propagated by calculating ΔK as a function of crack size and cyclic stress range. The accumulated number of cycles required to grow from the initial detectable defect to the critical condition was then converted into an equivalent fatigue life using the operational pressure-cycle spectrum. The resulting value represents a conservative estimate of the inspection-to-failure margin for the analysed scenario.

This approach allows the effect of material grade, pipeline geometry, operating pressure and hydrogen fraction to be compared consistently across the case matrix. However, the calculated fatigue lives should be interpreted as screening-level results. Pipeline-specific fatigue assessments would require actual pressure histories, material-specific fatigue crack growth data, detailed flaw characterisation and inspection performance information.

The research leading to these results has received funding from Horizon Europe, the European Union's Framework Programme for Research and Innovation under grant agreement n° 101111888.

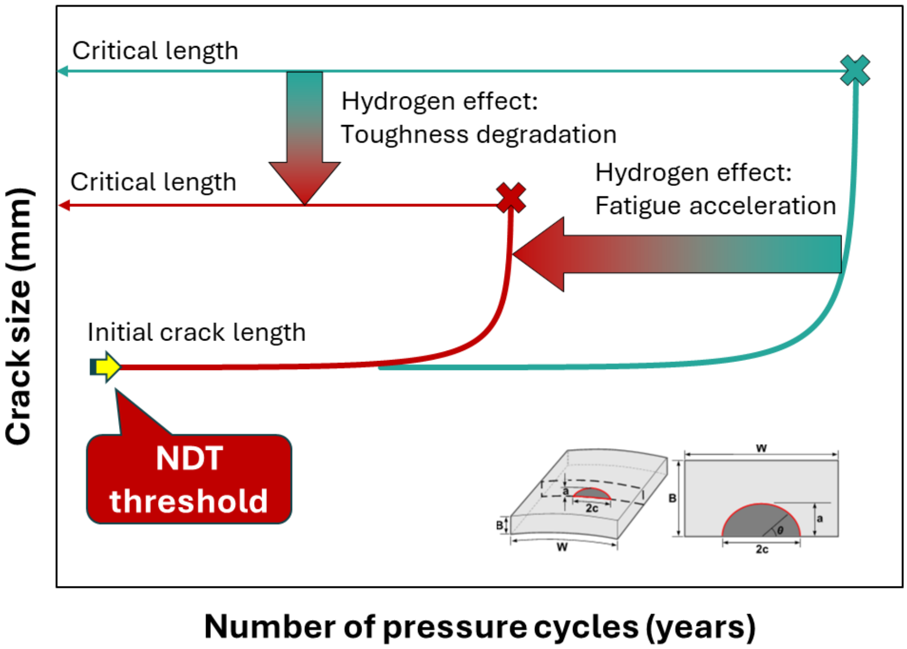

Figure 2 Hydrogen effects on fatigue lifetime assessment.

2.2.2.1 Operational pressure fluctuations

The fatigue-life calculation is governed by the cyclic stresses generated by pressure fluctuations during pipeline operation. In conventional natural gas systems, long-term pressure records are available and provide a realistic representation of operational loading conditions.

A single real natural-gas operational pressure history for period of one year was used as the reference loading spectrum for all pipeline configurations (see Figure 3). The original history was associated with pipeline of nominal pressure of 60 bar and the recorded pressure fluctuation spanned over a pressure range from approximately 48.7 to 67.9 bar, with a mean pressure of 60.8 bar and a standard deviation of 3.1 bar. To be able to apply the recorded pressure variation to different nominal pressure pipelines, for each analysed nominal pressure level, P_{nom}, the complete pressure history was shifted according to:

$$P_{adjusted}(t) = P_{recorded}(t) + (P_{nom} - 60) \quad \text{Equation 4}$$

Because the same constant pressure offset is added to every point in the recorded history, the pressure differences between data points remain unchanged. Consequently, the pressure-cycle ranges and their occurrence counts are preserved, while the absolute mean, minimum and maximum pressure levels are shifted.

The adjusted pressure signal was converted into the corresponding hoop-stress history using Equation 3. The resulting stress-time signal was processed using rainflow cycle counting in accordance with ASTM E1049 [19], as illustrated in Figure 3. Each extracted cycle was characterised by its stress range, mean stress, load ratio, R, and number of occurrences. The original temporal sequence is not retained after rainflow processing; for the fatigue crack growth calculation, the extracted cycles were arranged in descending order of stress range.

The complete rainflow-counted spectrum was treated as one equivalent annual loading block. Within each block, the stress intensity factor ranges at the crack-depth and surface locations were calculated using the crack dimensions at the beginning of the block. The crack-growth contributions from the individual cycles were accumulated and both crack depth and surface length were updated at the end of the block. The annual block was repeated until the evolving crack reached the limiting FAD condition. The equivalent fatigue life was calculated by dividing the accumulated number of cycles by the total number of rainflow-counted cycles in the reference annual spectrum.

The research leading to these results has received funding from Horizon Europe, the European Union's Framework Programme for Research and Innovation under grant agreement n° 101111888.

This approach allows representative operational pressure fluctuations to be incorporated into the screening analysis while keeping the treatment of hydrogen effects within the material-degradation model. It should be noted that the resulting fatigue lives are dependent on the selected pressure history and should therefore be interpreted as screening-level indicators rather than absolute lifetime predictions for a specific pipeline.

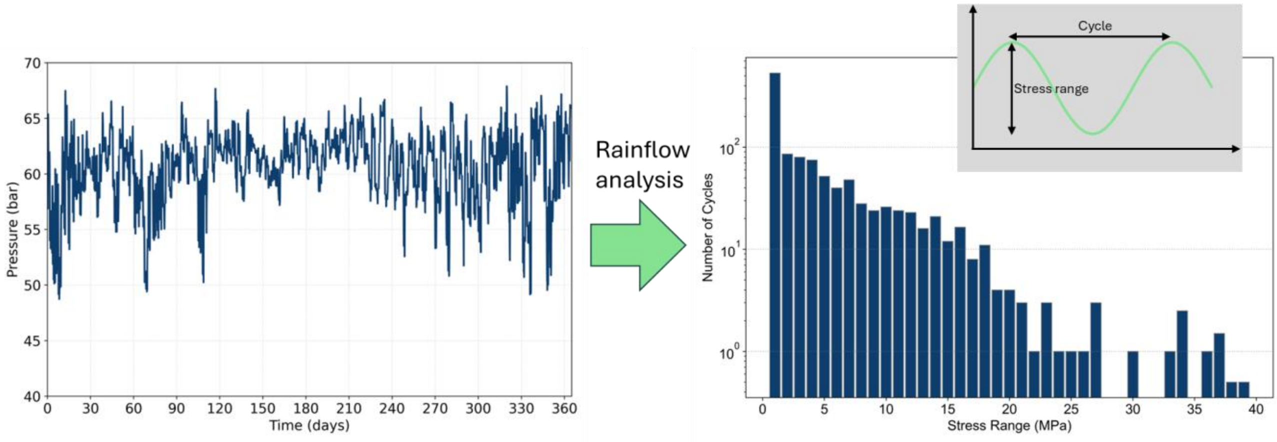

Figure 3 Derivation of stress range spectrum from operational pressure time series for FCG analysis.

2.2.2.2 Case matrix and sensitivity analysis

To evaluate the influence of key parameters on structural integrity, the assessment is implemented using a structured case-matrix approach in which material properties, pipeline geometry and operating conditions are systematically varied.

The parameter space is defined by varying four primary variables: material strength (API grade), pipeline geometry (OD and t), maximum operating pressure and hydrogen fraction in the transported gas. These variables directly control the crack driving force, fracture resistance and FCG behaviour.

The mechanical properties of the pipeline steels are defined according to the minimum strength requirements specified in ASME B31.12. The corresponding yield strength and ultimate tensile strength values are summarised in Table 1. These properties influence the structural integrity assessment through their role in the FAD formulation: the yield strength determines the reference stress ratio L_r, while the ultimate tensile strength defines the plastic collapse limit ($L_{r,max}$).

Table 1 Minimum strength requirements for API pipeline steels according to ASME B31.12.

Strength class (ISO)	Min. σ_y (MPa)	Min. σ_u (MPa)
X42 (L290)	290	415
X52 (L360)	360	460
X60 (L415)	415	520
X70 (L485)	485	570
X80 (L555)	555	625

The analysed pipeline geometries were selected to cover representative medium and large transmission pipeline sizes. The case matrix included different combinations of outside diameter and wall thickness, resulting in a range of diameter-to-thickness (OD/t) ratios. This parameter is relevant because, for a given internal pressure, higher diameter-to-thickness ratios generally lead to higher circumferential stresses and therefore higher crack-driving forces. The pipeline geometries considered in the assessment are listed in Table 2.

The research leading to these results has received funding from Horizon Europe, the European Union's Framework Programme for Research and Innovation under grant agreement n° 101111888.

Table 2 Pipeline geometries considered in the fatigue screening assessment.

OD (mm)	Wall thickness, t (mm)	Pipeline size category
273.0	5.2, 5.6, 6.4	Medium sizes
323.8	5.6, 6.4, 7.1	
406.4	5.6, 6.4, 7.1, 9.5	
508.0	7.1, 8.0, 9.5, 11.1	Large sizes
660.0	9.5, 11.1, 12.7, 14.3	
762.0	11.1, 12.7, 14.3, 17.5	
914.0	12.7, 15.9, 19.1, 20.6	

The operating conditions were defined by varying the nominal pressure level and the hydrogen fraction. Nominal pressure levels from 30 to 90 bar, in increments of 10 bar, were considered. The main screening matrix compared inert conditions with 100% hydrogen. Intermediate hydrogen fractions of 1%, 5%, 20%, 30% and 50% were additionally evaluated.

For the fatigue-life screening, the fracture toughness used to define the final critical condition was set to K_{mat}=55 MPa√m. This value was adopted as a conservative hydrogen-service screening threshold and was used consistently across the fatigue crack growth calculations. The purpose of this assumption was to avoid overestimating the propagation margin from the detectable defect to the critical condition.

Hydrogen-assisted fatigue crack growth was represented using the ASME B31.12 Code Case 220 formulation. This conservative curve was selected to provide a common basis for comparing different materials and geometries when material-specific fatigue crack growth data in hydrogen were not available for every steel grade and condition.

Residual stresses were considered through a conservative as-welded assumption, with secondary stresses taken as equal to the material yield strength. Since inspection capability depends on factors such as the technique employed, component geometry, access conditions, flaw orientation and operator qualification, a universal detectability threshold cannot be defined. The initial dimensions a_0=2 mm and $2c_0$=20 mm were therefore adopted as a technique-independent reference defect size for the preliminary screening assessment, broadly consistent with the typical inspection capabilities reported in Annex T of BS 7910. Accordingly, the calculated fatigue life represents the remaining propagation life from this assumed reference defect rather than from a universal or qualified detection limit.

The main input parameters adopted for the fatigue-life screening assessment are summarised in Table 3.

Table 3 Summary of input parameters used in the fatigue screening assessment.

Category	Parameter	Value(s)	Unit / Description
Operational condition	Nominal pressure	30–90 (step 10)	bar
	Hydrogen fraction	0, 1, 5, 20, 30, 50, 100	%
Material properties	K_{mat}	55	MPa√m
	FCG curve	ASME B31.12 CC220	mm/cycle
	ΔK_{th}	2	MPa√m
	Residual stress	As welded ($\sigma_{res} = \sigma_y$)	MPa
Initial defect definition	Initial crack depth, a_0	2	mm

The research leading to these results has received funding from Horizon Europe, the European Union's Framework Programme for Research and Innovation under grant agreement n° 101111888.

Initial surface length, $2c_0$	20	mm

It should be noted that the conservative value of K_{mat}=55 MPa√m was used only for the fatigue-life screening calculations. For the separate critical-defect and detectability assessment described in Section 2.2.3, representative fracture toughness values were derived from literature data for each API grade and environment. This distinction allows the fatigue-life analysis to remain conservative, while the critical-defect assessment captures the effect of material grade and hydrogen degradation on defect tolerance.

The purpose of the sensitivity analysis was to identify the combinations of material, geometry and operating condition that most strongly reduce the fatigue-life margin or bring detectable defects close to critical conditions. The results should therefore be interpreted as comparative screening outputs rather than as final acceptance criteria for specific pipelines.

2.2.3 Critical crack assessment

The critical crack assessment was performed to determine the flaw dimensions leading to the limiting structural condition for each material, geometry, pressure and environment considered in the screening matrix. Unlike the fatigue-life screening described in Section 2.2.2, which used a conservative fracture toughness, this assessment used representative fracture toughness values derived from literature data for each API grade and environment.

Surface flaws in pipelines are defined by two geometric parameters: crack depth, a, and surface length, 2c. Therefore, the critical condition cannot be represented by a single crack size. Instead, the assessment generates a critical defect envelope in the a-2c space. This envelope separates flaw dimensions that remain acceptable from those that reach the limiting FAD condition.

The assessment matrix included five API pipeline steel grades, from X42 to X80; the medium and large pipeline geometries defined in Table 2; operating pressures ranging from 30 to 90 bar; and two environmental conditions, namely inert and 100% gaseous hydrogen.

For each analysed configuration, the crack depth and surface length were systematically varied, and the corresponding FAD assessment point was calculated. The critical defect envelope was obtained when the assessment point reached the failure assessment line. This procedure was repeated for the selected API steel grades, pipeline geometries, operating pressures and environmental conditions.

Two environmental conditions were considered: inert conditions and pure gaseous hydrogen. The comparison between both environments allows the reduction in defect tolerance caused by hydrogen-degraded fracture toughness to be evaluated. The source data were grouped by nominal steel grade but not by production era, since manufacturing year, production route and service history were not consistently reported. Consequently, the representative median fracture toughness values summarised in Table 4 should be interpreted as pooled, grade-level screening properties rather than as values representative of either vintage or modern steels.

Table 4 Median fracture toughness values used for the critical crack assessment. Data from: [3–5,8,20–39].

Steel grade	K_{mat}, Inert (MPa√m)	K_{mat}, H_2 (MPa√m)
X42	162	98
X52	180	105
X60	142	96
X70	233	101
X80	252	104

The research leading to these results has received funding from Horizon Europe, the European Union's Framework Programme for Research and Innovation under grant agreement n° 101111888.

The calculated critical-defect envelopes were compared with the study-defined NDT reference dimensions selected with reference to the indicative inspection capabilities reported in Annex T of BS 7910. In this screening assessment, the detectability threshold was represented by an initial crack depth of a_0 = 2 mm and an initial surface length of $2c_0$ = 20 mm. This comparison provides an indication of whether a defect that is assumed to be detectable by inspection remains clearly below the critical condition or whether the detectable and critical domains become close.

The objective of this assessment was not to define inspection qualification limits, but to evaluate the available margin between representative detectable defects and critical defect conditions. Configurations in which the critical defect envelope approaches the detectability threshold were identified as requiring more detailed pipeline-specific assessment, including refined material properties, inspection capability, flaw sizing uncertainty and operational loading information.

As an independent design check, each material–geometry–pressure combination was also compared with the allowable pressure calculated according to ASME B31.12. The calculation used a design factor F=0.72, longitudinal joint factor E=1.0, temperature derating factor T=1.0, and the applicable hydrogen material performance factor H_f. This code-based pressure check was performed independently of the fracture-based inspection-screening classification.

The critical defect assessment therefore complements the fatigue-life screening. While the fatigue analysis estimates the time or number of cycles required for a detectable defect to reach a critical condition, the critical defect assessment evaluates how hydrogen exposure changes the critical flaw envelope itself. Together, both analyses provide a conservative screening basis for identifying repurposing scenarios where hydrogen service may reduce defect tolerance or inspection-to-failure margins.

2.3 Summary of fatigue life screening results

The results show that hydrogen-containing service reduces the calculated fatigue-life margin. This reduction is associated with the acceleration of fatigue crack growth under hydrogen exposure and with the reduction in the critical defect size used as the final condition of the propagation calculation. The magnitude of the reduction depends on the combined influence of operating pressure, hydrogen fraction, pipeline geometry and material grade.

The effect of hydrogen fraction is shown as an example in Figure 4 for a representative X42 pipeline geometry. For all pressure levels considered, the predicted fatigue life decreases as the hydrogen fraction increases. The largest reduction occurs when moving from inert or non-hydrogen conditions to hydrogen-containing conditions, while the additional decrease becomes more gradual as the hydrogen fraction approaches 100%. This trend indicates that even moderate hydrogen contents may have a relevant influence on fatigue crack growth margins under the conservative assumptions adopted in the screening assessment.

The research leading to these results has received funding from Horizon Europe, the European Union's Framework Programme for Research and Innovation under grant agreement n° 101111888.

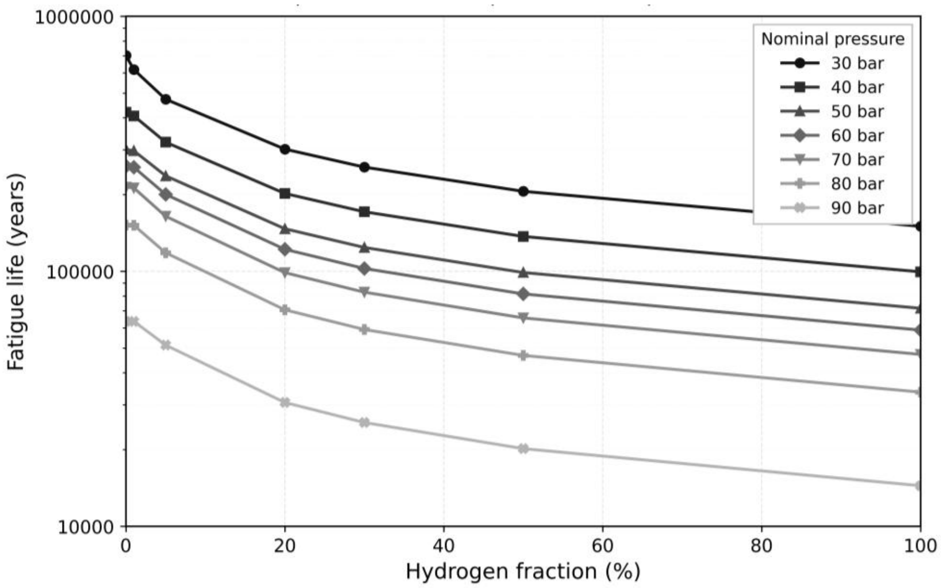

Figure 4 Example of influence of hydrogen fraction on fatigue life for an X42 pipeline.

The nominal pressure has a strong influence on the calculated fatigue life. For a given material and geometry, increasing the maximum pressure increases the circumferential stress range and therefore the stress intensity factor range driving crack propagation. As a result, higher pressure levels lead to shorter propagation lives. This effect is observed both in inert and hydrogen-containing conditions, although the reduction becomes more restrictive when hydrogen-assisted fatigue crack growth is considered.

The influence of pipeline geometry was assessed by comparing medium and large pipeline sizes at fixed nominal pressure of 40 bar. Figure 5 and Figure 6 compare the calculated fatigue lives under inert and 100% hydrogen conditions for X42. Geometries with higher OD/t generally develop higher hoop stresses and shorter fatigue lives. However, OD/t alone does not completely define the response because the absolute outside diameter, wall thickness and evolving crack geometry also influence the stress intensity factors and limiting FAD condition.

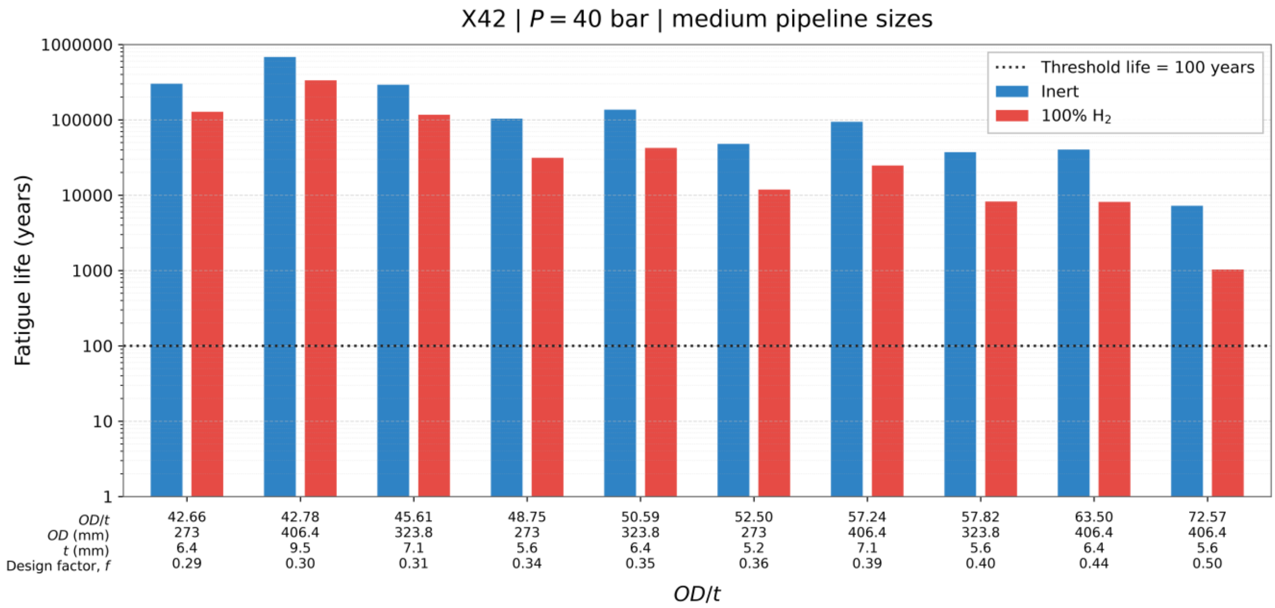

Figure 5 Effect of 100% H_2 on the fatigue life of X42 pipelines at nominal pressure of 40 bar for medium pipeline sizes.

The research leading to these results has received funding from Horizon Europe, the European Union's Framework Programme for Research and Innovation under grant agreement n° 101111888.

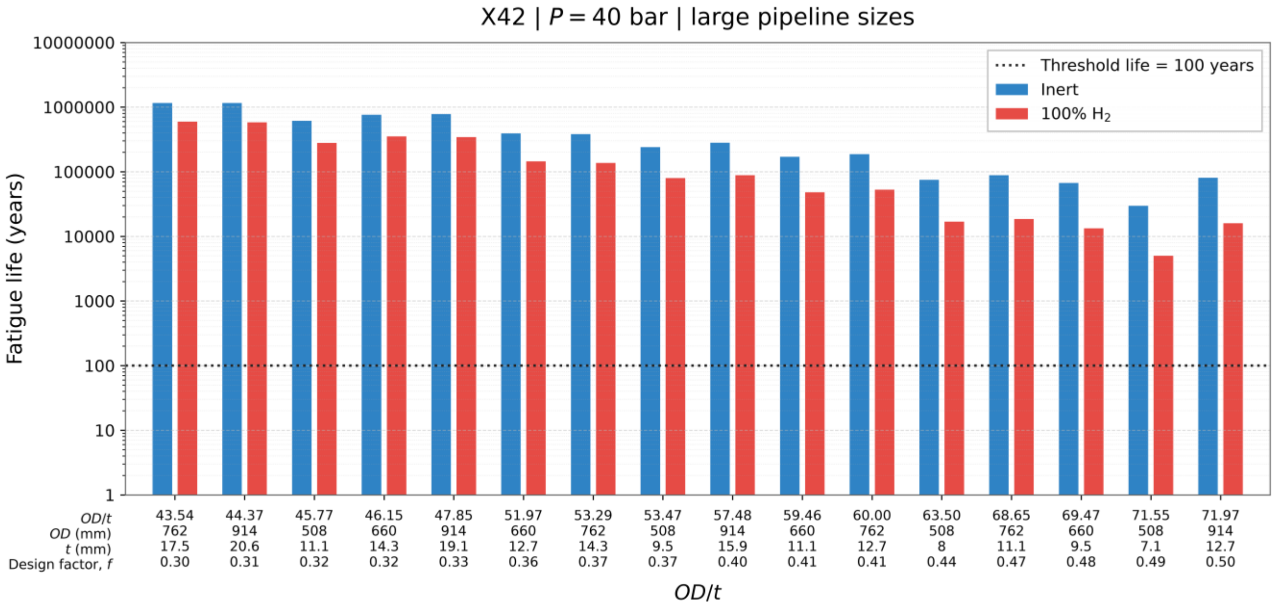

Figure 6 Effect of 100% H_2 on the fatigue life of X42 pipelines at nominal pressure of 40 bar for large pipeline sizes.

For both medium and large pipeline sizes, hydrogen exposure reduces the calculated fatigue life compared with inert conditions. At the nominal pressure represented in Figure 5 and Figure 6 (40 bar), however, all the analysed configurations remain approximately one order of magnitude or more above the adopted 100-year screening threshold. These figures should therefore be interpreted as illustrating the relative effect of hydrogen and geometry, rather than indicating proximity to the screening limit. Shorter fatigue lives are generally obtained for configurations with higher OD/t ratios, particularly where the initial crack depth represents a larger fraction of the wall thickness. Nevertheless, OD/t alone does not govern the response, since the absolute pipe dimensions, hoop-stress utilisation, evolving crack geometry and limiting FAD condition also influence the calculated life.

To condense the fatigue-life calculations into a project-level screening output, the highest analysed nominal pressure level for which the calculated propagation life remained at or above 100 years was identified for each material–geometry combination under 100% hydrogen. The results for the medium- and large-size matrices are presented in Figure 7 and Figure 8, respectively.

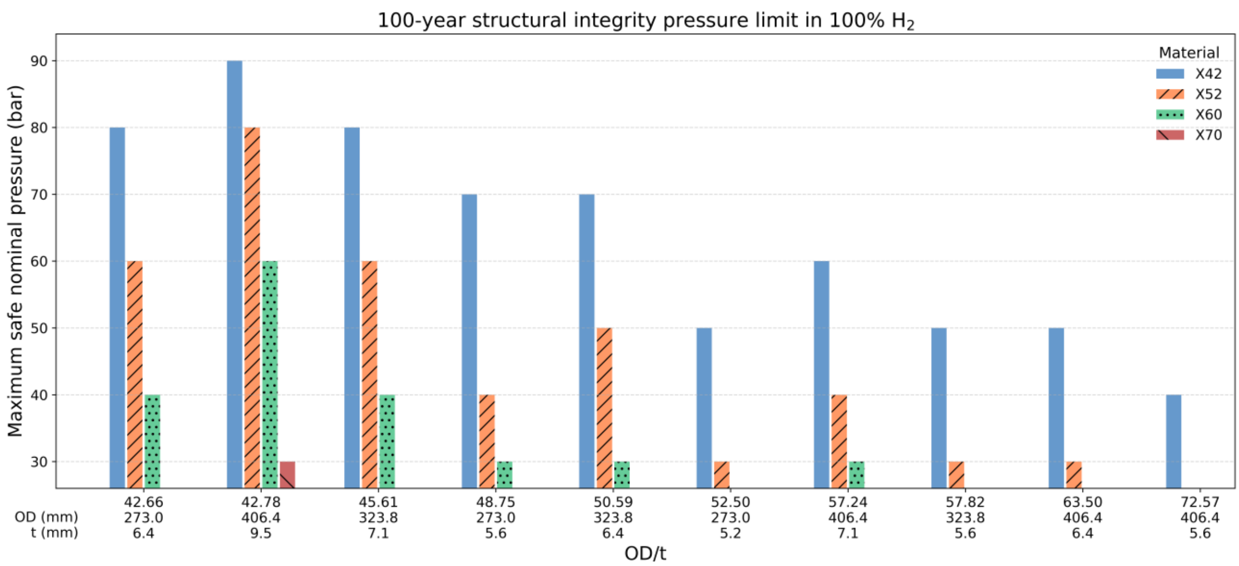

Figure 7. Highest analysed nominal pressure ensuring ≥100-year fatigue life for different API steels under 100% hydrogen and medium pipeline sizes.

The research leading to these results has received funding from Horizon Europe, the European Union's Framework Programme for Research and Innovation under grant agreement n° 101111888.

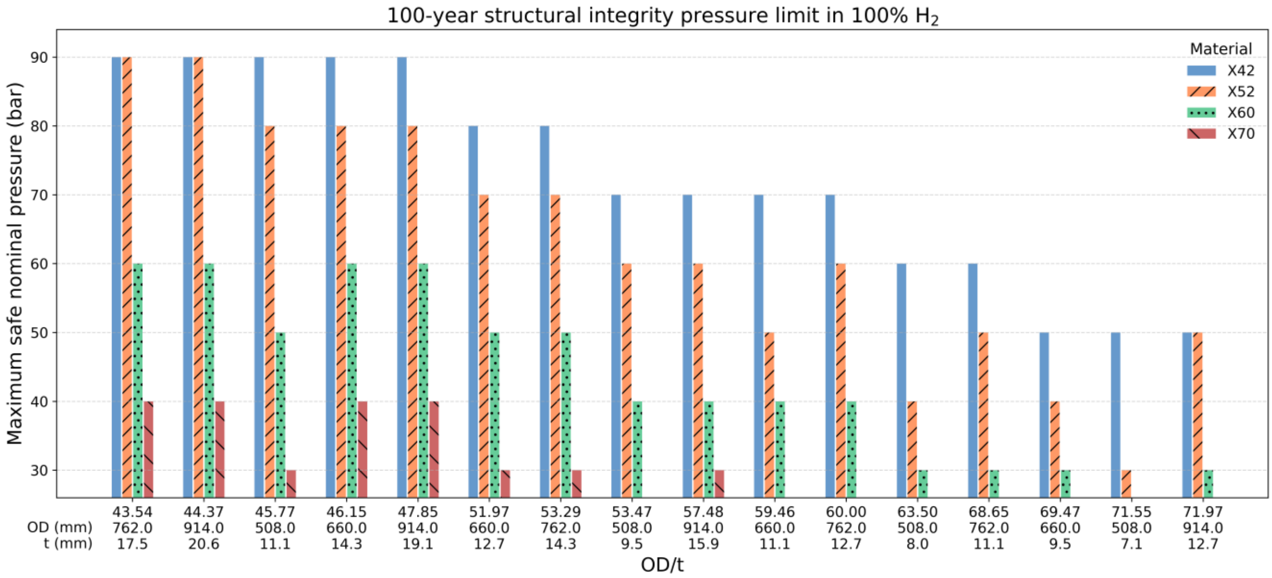

Figure 8. Highest analysed nominal pressure ensuring ≥100-year fatigue life for different API steels under 100% hydrogen and large pipeline sizes.

Figure 7 and Figure 8 should not be interpreted as code-based allowable pressures or MAOP values. They report the highest nominal pressure level within the discrete range analysed (30 to 90 bar in increments of 10 bar) that satisfies the adopted 100-year fatigue-life screening criterion. A value of 90 bar therefore indicates that the case remained above the threshold at the upper bound of the study, not that 90 bar constitutes its calculated limiting pressure.

The assumed residual-stress state plays an important role in interpreting the material-grade trends shown in Figure 7 and Figure 8. Residual stresses were introduced as secondary stresses, with an initial as-welded value equal to the YS of each grade. They therefore contribute principally to the secondary crack-driving force, increasing K_r, and also influence the effective load ratio used in the fatigue crack growth calculation, but they do not directly contribute to L_r. Consequently, higher-strength grades are assigned larger absolute residual stresses, which can reduce the calculated critical-defect size and fatigue propagation margin and may therefore be an important driver of the apparent material ranking.

This assumption is intentionally conservative. For comparison, neutron-diffraction measurements performed on the seam weld of a mechanically expanded UOE X65 linepipe reported maximum residual stresses of approximately 250 MPa, compared with a parent-material yield strength of 516 MPa, with most measured values below 50% of the yield strength.[40] Therefore, assigning the residual-stress magnitude as equal to the yield strength should be interpreted as an upper-bound screening assumption rather than as a representative measured residual-stress state. This conservatism should be considered when interpreting the material-grade ranking and the associated critical-defect and fatigue-life trends.

For medium pipeline sizes, shown in Figure 7, the admissible pressure generally decreases as the OD/t ratio increases. X42 exhibits the widest operating window, with several low-OD/t configurations remaining compatible with pressures up to the upper bound of the analysed range. X52 and X60 show progressively narrower admissible pressure ranges, particularly as the geometry becomes thinner-walled. Under the conservative fatigue-life screening assumptions, higher-strength grades such as X70 and X80 do not consistently provide an improved fatigue margin, despite their higher yield strength.

For large pipeline sizes, shown in Figure 8, the same general trend is observed, but the screening envelope becomes more restrictive for several configurations. Large-diameter geometries with relatively thin walls generate higher pressure-induced crack-driving forces, which reduces the pressure range compatible with a 100-year fatigue-life criterion. As a result, some material-geometry combinations that remain acceptable at lower pressures become limiting when pressure or OD/t ratio increases.

The research leading to these results has received funding from Horizon Europe, the European Union's Framework Programme for Research and Innovation under grant agreement n° 101111888.

The comparison between medium and large pipeline sizes indicates that the feasibility of hydrogen repurposing cannot be defined using pressure alone. The governing response depends on the combined effect of wall thickness, outside diameter, material grade and hydrogen-assisted fatigue crack growth. For the same nominal pressure, a geometry with a higher OD/t ratio may present a significantly lower propagation margin than a thicker-walled configuration. Therefore, pressure limits for hydrogen service should not be generalised without considering the specific pipeline geometry.

The apparent reduction in admissible pressure for higher-strength grades should also be interpreted with caution. These results do not imply that higher-grade pipeline steels are intrinsically unsuitable for hydrogen service. Rather, they reflect the conservative assumptions adopted in this screening analysis, including the use of a common hydrogen fatigue crack growth formulation, a conservative fracture toughness value for the fatigue-life endpoint, and minimum strength properties. In real pipeline assessments, material-specific fracture toughness, fatigue crack growth behaviour, weld condition and inspection performance could significantly modify the final margin.

From an engineering screening perspective, Figure 7 and Figure 8 separate the analysed cases into three practical groups. The first includes combinations that remain above the 100-year threshold throughout the nominal pressure range analysed. The second includes combinations that satisfy the criterion only up to an intermediate nominal pressure level and may therefore require refined assessment or pressure management. The third includes combinations that fail to reach the 100-year threshold even at the lowest nominal pressure considered. These groups support prioritisation for further assessment but do not constitute fitness-for-service acceptance categories.

Overall, the fatigue-life screening identifies nominal pressure level, pipeline geometry and hydrogen-assisted fatigue crack growth as the principal factors controlling the calculated propagation margin from the assumed reference defect to the limiting FAD condition. Figure 7 and Figure 8 should be interpreted as comparative screening maps for prioritising material-geometry combinations for more detailed assessment. They do not provide code-based pressure limits, MAOP values or pipeline-specific remaining-life predictions.

2.4 Summary of critical-defect assessment and inspection-screening results

The critical-defect and inspection-screening results evaluate the relationship between the critical flaw dimensions predicted by the FAD assessment and the assumed non-destructive testing (NDT) capability. Unlike the fatigue-life results presented in Section 2.3, which quantify crack propagation from an assumed detectable flaw to a critical condition, this section focuses on the position of the critical-defect envelope itself relative to the inspection-screening regions. For each material, geometry, pressure and environment included in the assessment matrix, critical-defect envelopes were calculated in terms of critical crack depth, a_{crit}, and critical surface length, $2c_{crit}$.

Figure 9 presents a representative comparison between the critical-defect envelopes obtained under inert and 100% H_2 conditions for X42 steel at OD/t=63.50 and 90 bar. The envelopes are superimposed on inspection-screening regions defined using a reference crack depth of a_{NDT}=2 mm and a reference surface length of $2c_{NDT}$=20 mm. These dimensions were selected with reference to the indicative inspection capabilities reported in Annex T of BS 7910. They are used as technique-independent screening assumptions and should not be interpreted as universal NDT detection limits, qualified inspection thresholds or probability-of-detection values.

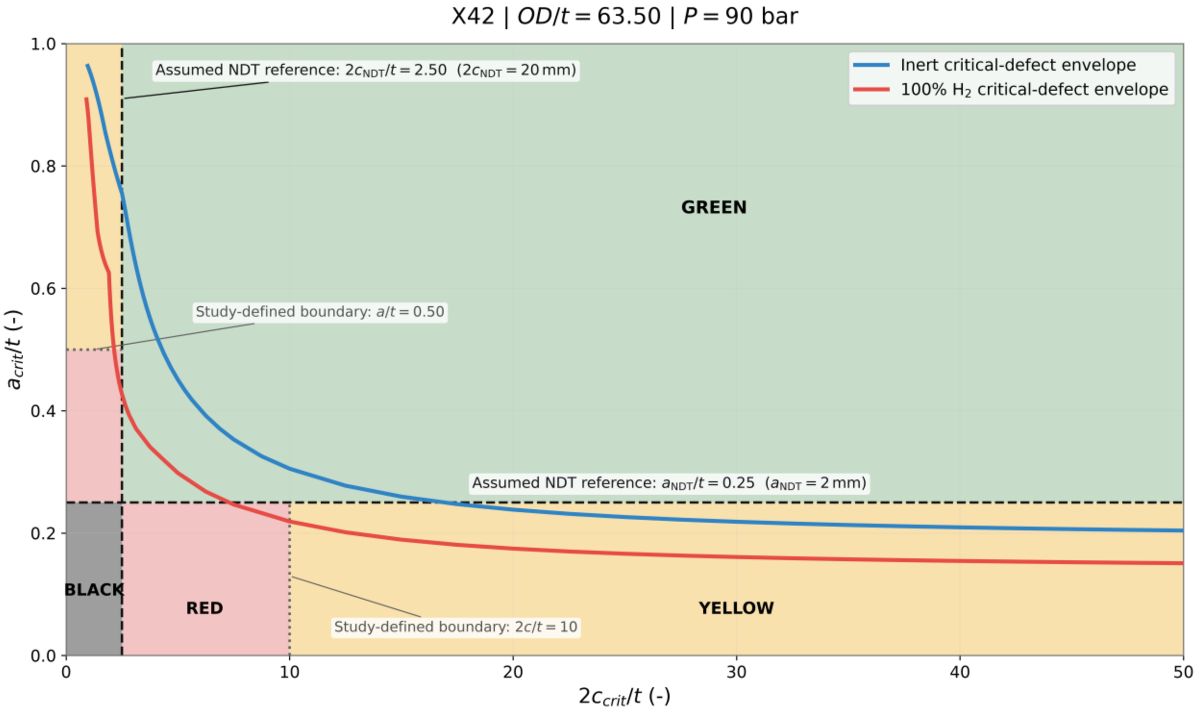

Figure 9. Example of critical-defect envelopes under inert and 100% hydrogen environments for X42 steel at OD/t = 63.50 and 90 bar (OD = 508, t = 8 mm).

The coloured background in Figure 9 classifies individual points of the critical-defect envelope. Black represents the fully sub-threshold region, in which both crack depth and surface length are below their respective NDT reference dimensions. Green represents the opposite condition, in which both dimensions equal or exceed their reference values. Red and yellow subdivide the two partial-detectability regions, where only one of the characteristic flaw dimensions exceeds its reference value. Red identifies conditions closer to the fully sub-threshold region, whereas yellow identifies conditions in which the dimension exceeding its reference value is geometrically more pronounced. Yellow therefore represents a lower relative inspection concern than red, but it does not imply guaranteed detection because the other characteristic dimension remains below its assumed reference value.

Within these partial-detectability regions, red and yellow were separated using study-defined geometric thresholds of $a/t=0.5$ and $2c/t=10$. For flaws with $2c<20$ mm and $a\geq2$ mm, the region is classified as red when $a/t<0.5$ and as yellow when $a/t\geq0.5$. Conversely, for flaws with $a<2$ mm and $2c\leq20$ mm, the region is classified as red when $2c/t<10$ and as yellow when $2c/t\geq10$.

Please note that these thresholds are not based on inspection capability, published acceptance criteria, BS 7910 limits, or probability-of-detection data. The value $a/t=0.5$ was selected as a physically interpretable depth marker corresponding to a crack depth equal to half the wall thickness. The value $2c/t=10$ was selected as an aspect-ratio marker for elongated flaws, providing a reproducible separation between partial-detectability cases with a relatively limited surface extent and those with a more pronounced longitudinal extent. The two values were adopted as fixed visualization conventions after reviewing the normalized critical-defect envelopes across the assessment matrix.

They are therefore intended only to provide a consistent and reproducible visual classification for comparative screening. Changing these study-defined thresholds would modify the red yellow subdivision, but would not modify the calculated critical-defect envelopes or the underlying FAD results.

To summarise the large number of critical defect envelopes generated in the parametric study, the results were condensed into traffic-light detectability maps. These maps provide a practical screening representation of the combined influence of material grade, geometry and pressure on the margin between critical and detectable

The research leading to these results has received funding from Horizon Europe, the European Union's Framework Programme for Research and Innovation under grant agreement n° 101111888.

defects. To assign a single traffic-light colour to each complete critical-defect envelope, the short-flaw and shallow-flaw branches were considered together. A case was classified as black if any part of the envelope entered the region where both flaw dimensions are below the assumed NDT reference values. Otherwise, the overall colour was assigned from the two branch classifications: red was used for red-red or red-yellow combinations, yellow for red-green or yellow-yellow combinations, and green for green-green or green-yellow combinations.

Figure 10 and Figure 11 present the resulting traffic-light maps for the medium- and large-diameter pipeline matrices, respectively. Each cell represents one combination of material grade, OD/t and operating pressure in 100% H_2. Black indicates the highest inspection concern, red a high concern, yellow an intermediate concern and green a low concern under the adopted screening assumptions. These categories provide a relative ranking for further assessment and should not be interpreted as direct fitness-for-service acceptance criteria.

The ASME B31.12 check provides an additional and overriding design-screening layer. The allowable pressure was calculated using a design factor F=0.72, a longitudinal joint factor E=1.0, a temperature derating factor T=1.0, and the hydrogen material performance factor H_f prescribed according to pipe grade and pressure. Over the pressure range considered in this study (30-90 bar), the adopted H_f values were 1.0 for X42 and X52, 0.874 for X60 and X70, and 0.776 for X80.

Cells for which the analysed pressure exceeds the calculated allowable pressure are displayed in grey with diagonal hatching, irrespective of their underlying inspection-screening colour. The grey-hatched category therefore identifies combinations that should first be excluded by the adopted design-pressure check, while the remaining-coloured cells retain the inspection-screening classification described above. The grey hatching takes precedence over the traffic-light colour and identifies combinations for which the analysed pressure exceeds the calculated ASME B31.12 allowable pressure, this means that these pipelines would never have been built for either natural gas or hydrogen.

The research leading to these results has received funding from Horizon Europe, the European Union's Framework Programme for Research and Innovation under grant agreement n° 101111888.

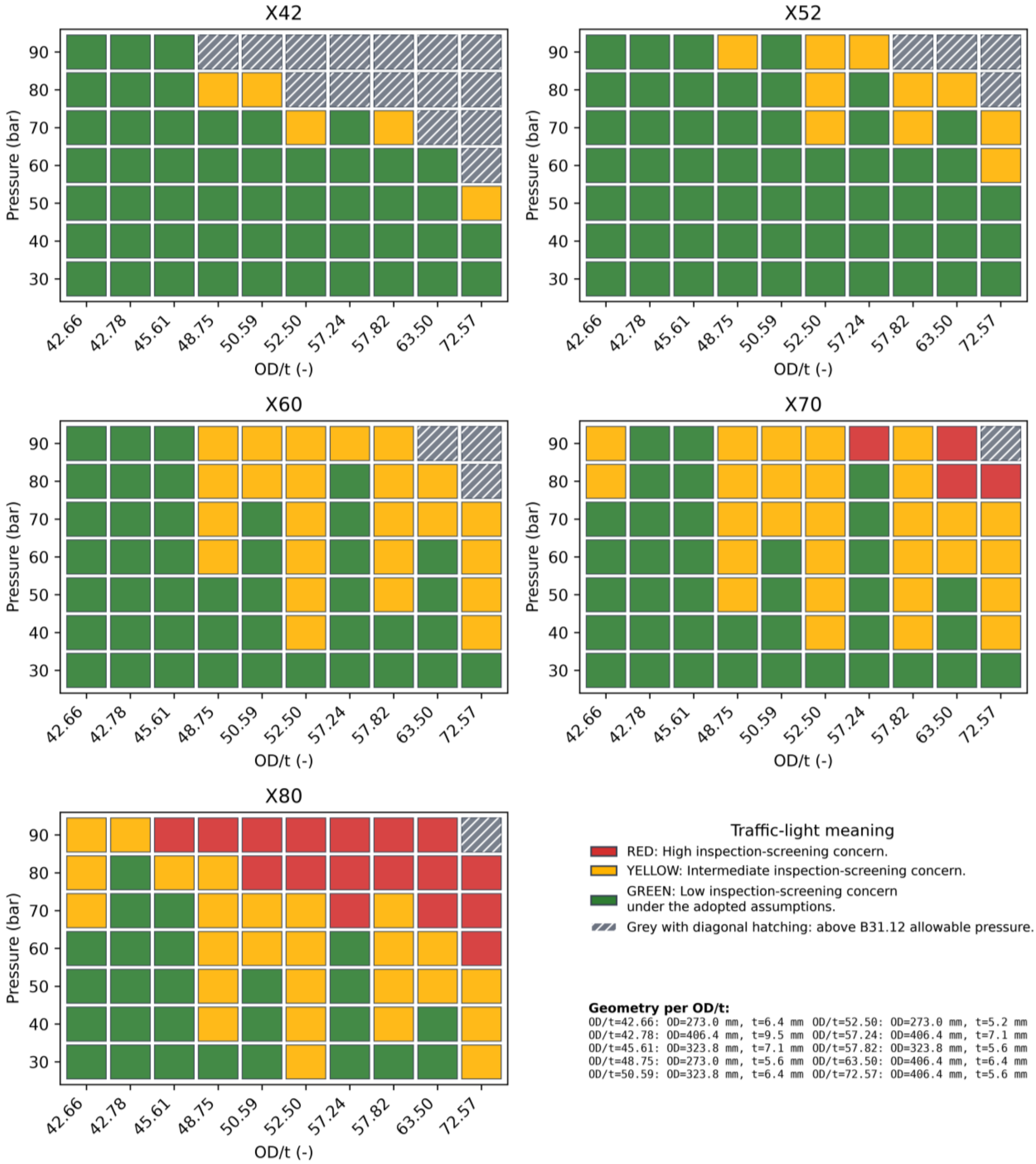

Figure 10. Case-level inspection-screening priorities in 100% H_2 for the medium-diameter pipeline matrix. Grey diagonal hatching identifies combinations exceeding ASME B31.12 design conditions.

The research leading to these results has received funding from Horizon Europe, the European Union's Framework Programme for Research and Innovation under grant agreement n° 101111888.

Figure 11. Case-level inspection-screening priorities in 100% H_2 for the large-diameter pipeline matrix. Grey diagonal hatching identifies combinations exceeding ASME B31.12 design conditions.

Figure 10 and Figure 11 show that operating pressure is the main parameter driving the transition towards higher inspection-screening concern. Green cells dominate at the lower pressure levels, whereas yellow and red cells become more frequent at higher pressures as the critical-defect envelopes move towards smaller flaw dimensions. Grey-hatched cells also become more frequent at the highest pressures and for the slenderer geometries, reflecting the independent ASME B31.12 allowable-pressure check. Higher OD/t values generally reduce the available integrity margin, although the trends are not strictly monotonic because the response depends on the combined effects of outside diameter, wall thickness, material properties, fracture toughness and pressure.

The research leading to these results has received funding from Horizon Europe, the European Union's Framework Programme for Research and Innovation under grant agreement n° 101111888.

In the medium-diameter matrix shown in Figure 10, the final displayed classification comprises 212 green cells, 93 yellow cells, 21 red cells and 24 grey-hatched cells out of the 350 combinations analysed. No black cell is visible in the map because the black underlying classification is covered by the overriding grey-hatching criterion. The higher inspection-screening concerns are concentrated mainly at 80 and 90 bar. X42 contains several yellow cells and a number of grey-hatched cells, but no visible red or black cells. The visible red classifications are concentrated mainly in X70 and X80, particularly at the highest pressures, and represent pressure-compliant combinations for which the detectability margin remains a relevant concern.

The large-diameter matrix shown in Figure 11 contains 416 green cells, 77 yellow cells, 8 red cells and 59 grey-hatched cells among the 560 combinations analysed. The transition towards higher concern is again concentrated at the upper pressure levels, although the large-diameter matrix contains a higher proportion of green cells than the medium-diameter matrix. X42 and X52 remain entirely green among the non-hatched cells; their higher-pressure and more slender configurations are instead mainly covered by the ASME B31.12 design check. The remaining visible yellow and red classifications occur principally for X60, X70 and X80 at higher pressures, with the most severe visible cases concentrated in the X70 and X80 matrices.

The grey hatching takes precedence over the traffic-light colour and identifies combinations for which the analysed pressure exceeds the calculated ASME B31.12 allowable pressure. Consequently, the displayed colours describe the inspection-screening concern only for pressure-compliant combinations, whereas grey cells should first be excluded under the adopted design-pressure criterion. The two assessments therefore provide complementary information: the traffic-light classification evaluates the relationship between the critical-defect envelope and the assumed NDT reference dimensions, while the grey hatching identifies combinations that do not satisfy the independent design-pressure check. Some grey-hatched cells would otherwise have a low or intermediate underlying inspection-screening classification, demonstrating that compliance with the inspection criterion does not imply compliance with the allowable-pressure requirement.

Overall, the maps provide a screening tool for distinguishing pressure-compliant combinations with different levels of inspection concern from combinations that exceed the adopted ASME B31.12 allowable pressure. Green should be interpreted as the lowest relative inspection-screening concern among the pressure-compliant cases under the adopted assumptions, rather than as proof of structural safety. Yellow and red cells identify progressively higher inspection-screening priorities, while grey-hatched cells should first be excluded or reassessed from the design-pressure perspective. The maps do not replace pipeline-specific fracture-mechanics calculations, qualified inspection procedures, detailed flaw-sizing assessments or a complete code-compliance evaluation.

2.5 Implications, limitations and recommendations for hydrogen repurposing

The structural-integrity assessment provides a conservative screening framework for identifying the pipeline configurations for which hydrogen repurposing may require pressure management, improved inspection capability or a more detailed engineering assessment. The results demonstrate that repurposing feasibility cannot be determined from material grade or operating pressure alone, but depends on the combined influence of pressure, pipe geometry, material properties, fatigue crack growth, fracture resistance and inspection capability.

The fatigue-life assessment shows that hydrogen-containing service reduces the calculated propagation margin from the assumed reference defect to the limiting FAD condition. Within this part of the assessment, a common conservative fracture toughness of 55 MPa√m was used for all environments; consequently, the effect of hydrogen fraction on the calculated life is introduced through the adopted hydrogen-assisted fatigue crack growth formulation. Higher nominal pressures and larger OD/t ratios generally produce shorter fatigue lives, although the response is not governed by OD/t alone because the absolute pipe dimensions and evolving crack geometry also influence the crack-driving force. The pressure values reported in Figures 7 and 8 should therefore be interpreted only as the highest discrete nominal pressure analysed for which the adopted 100-year screening criterion was satisfied. They are not code-based allowable pressures, MAOP values or pipeline-specific remaining-life predictions.

The research leading to these results has received funding from Horizon Europe, the European Union's Framework Programme for Research and Innovation under grant agreement n° 101111888.

The apparent material-grade trends should also be interpreted in the context of the adopted assumptions. In particular, the as-welded residual stress was conservatively taken as equal to the yield strength of each grade, while a common fatigue crack growth formulation and the same fatigue endpoint toughness were applied across the material matrix. Higher-strength grades therefore do not necessarily exhibit a larger calculated fatigue margin. This result should not be interpreted as evidence that these grades are intrinsically less suitable for hydrogen service, but as an indication that their relative performance is sensitive to residual stress, fracture toughness, weld condition and material-specific fatigue crack growth behaviour.

The critical-defect assessment addresses a different but complementary aspect of structural integrity. In this analysis, material- and environment-specific fracture toughness values were used to determine the critical-defect envelopes. Hydrogen exposure can therefore shift these envelopes towards smaller flaw dimensions through the reduction in fracture resistance, although the magnitude of this effect depends on the material grade, geometry and applied pressure. The traffic-light classification compares the resulting critical flaw dimensions with the adopted NDT reference dimensions and provides a relative indication of inspection-screening concern. Green represents the lowest concern, yellow an intermediate concern, red a high concern and black the most severe underlying inspection-screening condition under the adopted assumptions. However, the traffic-light classification is subject to the independent ASME B31.12 design-screening overlay described below. These categories are therefore intended as screening priorities and should not be interpreted as fitness-for-service acceptance criteria or as confirmation that a green case is structurally safe.

The ASME B31.12 allowable-pressure check provides an overriding design-screening layer. Grey-hatched cells correspond to combinations for which the analysed pressure exceeds the calculated allowable pressure and should therefore be screened out first under the adopted design assumptions, irrespective of their underlying inspection-screening classification. The remaining unhatched coloured cells represent pressure-compliant combinations and retain their traffic-light classification. In the matrices shown in Figures 10 and 11, all underlying black cases are covered by the overriding grey-hatching; consequently, no black cell is visible in the final maps. The pressure-compliant inspection concerns are therefore represented by unhatched yellow and red cells, which identify combinations requiring progressively more detailed assessment of inspection capability and critical-defect tolerance. Conversely, some grey-hatched cells would otherwise have a green or yellow underlying classification, demonstrating that a low inspection concern does not imply compliance with the allowable-pressure requirement. Compliance with the ASME B31.12 allowable-pressure check likewise does not, by itself, demonstrate that the inspection-to-failure margin is adequate. The combined results suggest a sequential approach to repurposing decisions. Compliance with the applicable design-pressure requirements should first be established. For the remaining combinations, the fatigue propagation margin and the relationship between the qualified inspection capability and the critical-defect envelope should then be evaluated. Cases that satisfy the design-pressure check but fail the adopted fatigue-life criterion, or retain an unhatched red or black inspection classification, should be prioritised for pipeline-specific engineering critical assessment. Yellow cases should also be reviewed where inspection performance, material properties or loading conditions are uncertain.

The screening results are subject to several limitations. The fatigue calculations use a common conservative fracture toughness, an adopted threshold of $\Delta K_{th} = 2$ MPa$\sqrt{m}$ and a hydrogen-assisted fatigue crack growth formulation intended for comparative screening rather than material-specific life prediction. The loading spectrum is derived from a representative natural-gas pressure history and is treated as a repeated annual block; it may therefore not reproduce the pressure cycling of a future hydrogen network or a specific pipeline. The critical-defect calculations use pooled, literature-derived median fracture toughness values for each grade and environment rather than measurements from the assessed assets. The calculations also assume semi-elliptical internal axial surface flaws, minimum material strength properties and a conservative as-welded residual-stress condition.

In addition, the reference dimensions of a = 2 mm and 2c = 20 mm are technique-independent screening assumptions derived with reference to Annex T of BS 7910. They are not qualified detection limits or probability-of-detection values. Actual inspection performance will depend on the inspection method, defect morphology and orientation, pipe geometry, access conditions, sizing uncertainty and qualification procedure.

The research leading to these results has received funding from Horizon Europe, the European Union's Framework Programme for Research and Innovation under grant agreement n° 101111888.

The red-yellow boundaries and the resulting case-level colour classifications are likewise study-specific screening conventions rather than acceptance criteria prescribed by BS 7910.

Pipeline-specific repurposing assessments should therefore use measured material properties wherever possible, including fracture toughness and fatigue crack growth data representative of the base material, weld metal and heat-affected zone in the relevant hydrogen environment. They should also incorporate actual pressure histories, a justified residual-stress distribution, qualified inspection performance and flaw-sizing uncertainty. Where the calculated margin is limited, potential mitigation measures include reducing operating pressure, improving inspection capability, shortening inspection intervals, applying more restrictive defect acceptance criteria or undertaking repair or replacement.

Overall, the assessment provides a structured basis for ranking repurposing scenarios and identifying where additional integrity work is required. It does not establish universal hydrogen blending limits or provide final acceptance decisions for individual pipelines. A favourable screening result indicates a lower relative concern under the adopted assumptions, whereas an unfavourable result identifies the need for additional evidence or mitigation before hydrogen-containing service is considered.

The research leading to these results has received funding from Horizon Europe, the European Union's Framework Programme for Research and Innovation under grant agreement n° 101111888.

3 Effect of gas quality and composition on hydrogen embrittlement

3.1 Introduction

Hydrogen embrittlement is one of the main integrity concerns associated with the exposure of pipeline steels to hydrogen-containing gaseous environments. In pipeline steels, hydrogen exposure has been associated with reductions in ductility-related properties, including elongation and reduction of area, as well as decreases in fracture toughness and accelerated fatigue crack growth rates (FCGR) under cyclic loading conditions.[3,41,42] Increasing hydrogen partial pressure generally increases hydrogen uptake and hydrogen embrittlement susceptibility in pipeline steels, although the severity of degradation may also depend on the surrounding gas composition and testing conditions.

While numerous studies have investigated hydrogen-assisted degradation in simplified H_2/N_2 or H_2/CH_4 mixtures, the influence of additional natural gas components and impurities remains insufficiently understood. In particular, species such as CO_2, CH_4, CO, H_2S, N_2 and higher hydrocarbons may alter hydrogen uptake and hydrogen-assisted degradation through competitive adsorption, surface interactions, transport kinetics and trapping effects.

3.2 Effect of gas components on hydrogen embrittlement (literature review)

Some of the classic foundational studies on the problem of hydrogen embrittlement of pipeline steels investigated the interaction of different gaseous species with iron. The study showed that different gases exhibit markedly different adsorption behaviours and therefore strongly different effects on hydrogen embrittlement susceptibility. In particular, O_2, CO, SO_2, COS, N_2O and C_2H_4 were found to adsorb strongly on iron surfaces and inhibit hydrogen uptake, whereas CO_2, CH_4 and C_2H_6 exhibited weak or negligible interaction with the steel surface. The authors attributed this behaviour to the limited adsorption and dissociation capability of these gases on iron surfaces, which prevented them from effectively blocking hydrogen adsorption sites and hydrogen ingress into the material.[43,44]

Recently, a detailed review emphasized that the effect of gaseous additives cannot be generalized independently of the testing methodology and operating conditions. [45]The review highlighted that reported inhibition or promotion effects strongly depend on parameters such as hydrogen partial pressure, additives partial pressure, testing conditions and material microstructure. The authors further acknowledge the apparently contradictory results in the literature and related them to the wide variation in experimental methods and loading conditions used across different studies.

In the following sections, the main findings available in the literature regarding the influence of the principal gas components and impurities present in hydrogen-containing natural gas mixtures on the hydrogen embrittlement behaviour of pipeline steels are reviewed.

3.2.1 Role of CH_4

The available literature on CH_4 effect on hydrogen embrittlement is rather consistent, with most studies reporting either a weak inhibitory effect or little to no significant effect of CH_4 on hydrogen embrittlement in steels. [43,45] A recent Density Functional Theory (DFT) study investigating the dissociative adsorption of H_2 and CH_4 at high-angle grain boundaries in pipeline steels showed that CH_4 can exert a weak competitive adsorption effect on hydrogen adsorption, although it could not completely prevent hydrogen dissociative adsorption from occurring.[46]

An interesting study relevant to the conditions of the present work investigated the effect of CH_4 on the hydrogen embrittlement susceptibility of X80 pipeline steel in hydrogen-blended natural gas environments by means of Slow Strain Rate Testing (SSRT). The experiments were conducted at a total pressure of 10 MPa, with a constant hydrogen concentration of 20 vol%, while the CH_4 content was varied from 0 to 40 vol%. The results showed that increasing CH_4 concentration progressively reduced the hydrogen embrittlement susceptibility of X80 steel, however, the inhibition effect tended to stabilize once the CH_4 content exceeded approximately 20 vol%. The authors attributed this behaviour to competitive adsorption between CH_4 and H_2

The research leading to these results has received funding from Horizon Europe, the European Union's Framework Programme for Research and Innovation under grant agreement n° 101111888.

on the iron surface, where CH_4-derived adsorbed species reduced the availability of dissociative adsorption sites for hydrogen and consequently decreased hydrogen ingress into the steel. [47]

3.2.2 Role of N_2

N_2 is generally considered an inert component in hydrogen-containing gaseous environments. The available literature on the role of N_2 in hydrogen embrittlement in hydrogen containing blends is limited. Most studies use N_2 primarily as a reference media for comparison with hydrogen-containing atmospheres or balance gas in mixtures. However, recent studies investigated the effect of total gas pressure on the fatigue crack growth behaviour of X80 and GB20# pipeline steels in H_2/N_2 mixtures. The experiments compared pure hydrogen environments with H_2/N_2 mixtures at identical hydrogen partial pressures but different total pressures. The results showed higher FCGR values in the high-pressure H_2/N_2 mixtures than in pure hydrogen at the same hydrogen partial pressure, indicating enhanced hydrogen-assisted degradation under elevated total gas pressure conditions. Simulations suggested that increasing the overall gas pressure through the addition of N_2 increased the kinetic energy and velocity of hydrogen molecules and reduced the hydrogen dissociation time at the iron surface, thereby promoting hydrogen entry into the material.[48,49] Nevertheless, experimental evidence regarding a direct effect of N_2 on hydrogen embrittlement susceptibility remains scarce.

3.2.3 Role of CO_2

The influence of CO_2, on hydrogen embrittlement in blends remains insufficiently understood. The literature reports markedly different effects, ranging from enhanced crack growth and embrittlement susceptibility to inhibiting or negligible effects on hydrogen uptake and hydrogen-assisted degradation. Thus, the effect of CO_2 appear to be strongly dependent on the material system, gas composition, pressure conditions, and testing methodology.

Early studies generally reported that CO_2 exhibited weak or negligible interaction with iron surfaces and therefore had little effect on hydrogen adsorption or hydrogen-assisted crack growth.[43,44,50]

A recent study investigated the effect of CO and CO_2 impurities on the hydrogen embrittlement susceptibility of X52 pipeline steel using SSRT, hydrogen permeation and Thermal Desorption Spectroscopy, The tests were conducted at a total pressure of 4 MPa (40 bar), with a constant H_2 partial pressure of 2 MPa (20 bar), while the CO_2 partial pressure was varied from 0 to 1 MPa (0–10 bar). The results showed that CO_2 reduced hydrogen embrittlement susceptibility, and that the inhibitory effect increased with increasing impurity partial pressure. In the CO_2-containing environments, the reduction of area and elongation gradually increased with increasing CO_2 partial pressure, while the hydrogen embrittlement index decreased. The authors attributed this behaviour to competitive surface adsorption between CO_2 and H_2, which reduced hydrogen surface coverage and hydrogen uptake into the material. However, it should be noted that the CO_2 partial pressure range investigated in this study (up to 1 MPa, 10 bar) was significantly higher than the CO_2 partial pressure used in the present work (~0.08 MPa, 0.8 bar). [51]

In contrast to the reported inhibitory effect of CO_2, fatigue crack growth experiments performed on L360/X52 pipeline steel in 6 MPa H_2 environments showed that the addition of 2.5% CO_2, (partial pressure of approximately 0.15 MPa), slightly promoted hydrogen embrittlement. The fatigue crack growth rates in the CO_2-containing environment were comparable to or slightly higher than those measured in pure hydrogen. Hydrogen permeation measurements further showed that the presence of CO_2 shortened the hydrogen breakthrough time, indicating that CO_2 facilitated hydrogen ingress into the steel. The authors attributed this behaviour to a reduction in the activation barrier for hydrogen dissolution and migration from the surface into the subsurface region, which increased the hydrogen concentration at the crack tip and accelerated fatigue crack propagation. [52]

Shang et al. showed that, during fatigue crack growth in low-carbon steel, Natural gas/H_2 mixtures hydrogen embrittlement can be more severe than pure H_2, and they attributed this behaviour to a CO_2–H_2 synergistic effect.[53] Similar observations were also reported by Cui et al. for high CO_2 concentrations (5- 40 vol% CO_2), where the addition of CO_2 to high-pressure hydrogen-containing gas mixtures increased the hydrogen embrittlement susceptibility of X65 pipeline steel.[54]

The research leading to these results has received funding from Horizon Europe, the European Union's Framework Programme for Research and Innovation under grant agreement n° 101111888.

In a later study on X80 pipeline steel, it was observed that CO_2 enhanced the fatigue crack growth of X80 steel in hydrogen-containing environments, and that the degree of acceleration increased with increasing CO_2 content. The FCGR tests were conducted at a total pressure of 0.4 MPa, with a constant H_2 partial pressure of 0.04 MPa, while the CO_2 partial pressure was varied from 0.0002 to 0.02 MPa, corresponding to CO_2 contents between 0.005 and 0.5 vol%. DFT calculations suggested that the adsorbed CO_2 molecules significantly accelerated the migration of hydrogen atoms from the surface into the subsurface region, thereby promoting hydrogen uptake into the steel.[55]

To explain the complex effect of CO_2 on hydrogen embrittlement FCGR studies demonstrated that CO_2 promoted hydrogen-assisted crack growth in low-pressure hydrogen-containing environments, whereas the magnitude of this effect became significantly less pronounced at higher hydrogen pressures. In X80 and GB20# pipeline steels tested under 10 MPa total pressure with 10 vol% H_2, the accelerating effect of CO_2 on FCGR was substantially weaker than that previously observed under 0.4 MPa conditions at the same gas composition. The authors attributed this pressure dependence to the increased hydrogen surface coverage at high hydrogen pressures, which reduced the adsorption rate of CO_2 on the steel surface and limited its ability to further accelerate hydrogen uptake into the material. Thus, the influence of CO_2 strongly depends on the testing conditions, hydrogen pressure, material, and crack growth regime.[56]

Recent work also provides a possible framework for explaining the contradictory literature regarding the role of CO_2 in hydrogen embrittlement. Using SSRT, FCGR, hydrogen permeation experiments, and first-principles molecular dynamics simulations on high-purity iron, the authors showed that the effect of CO_2 is non-monotonic and strongly dependent on CO_2 partial pressure. At relatively low CO_2 partial pressures (0.002–0.2 MPa), CO_2 promoted hydrogen dissolution and subsurface migration, leading to increased hydrogen embrittlement. In contrast, at higher CO_2 partial pressures (0.4–0.6 MPa), CO_2 increasingly occupied surface adsorption sites, reducing hydrogen adsorption and permeation, which resulted in a partial inhibition of hydrogen embrittlement. The most severe embrittlement was observed at approximately 0.2 MPa CO_2 partial pressure. The authors therefore proposed that CO_2 exerts a dual effect on hydrogen embrittlement: promotion at low concentrations and inhibition at higher concentrations, depending on the balance between enhanced hydrogen dissolution and competitive surface site blocking. [57]

Overall, the available literature suggests that the effect of CO_2 on hydrogen embrittlement is strongly dependent on the testing conditions and gas environment. These observations indicate that the role of CO_2 cannot be considered universal and may depend on factors such as pressure, gas composition, material microstructure and the dominant hydrogen transport mechanisms involved.

3.2.4 Role of C_2H_6 and higher hydrocarbons

The available literature on C_2H_6 and higher hydrocarbons is limited. Early pioneering studies on gaseous inhibitors in hydrogen embrittlement reported that saturated hydrocarbons such as CH_4 and C_2H_6 exhibited little or no inhibition effect on hydrogen-assisted degradation of pipeline steels. Surface adsorption analyses showed that C_2H_6 did not adsorb significantly or dissociate on iron surfaces and therefore did not effectively block hydrogen adsorption or hydrogen uptake into the material. In contrast, unsaturated hydrocarbons such as C_2H_4 showed stronger interaction with iron surfaces and exhibited a more pronounced inhibition effect.[43,50]

A recent experimental study investigated the hydrogen embrittlement behaviour of X52, X60 and X70 pipeline steels in realistic natural gas/hydrogen mixtures under high-pressure gaseous conditions. The results showed that, at low hydrogen concentrations (<20 vol%), embrittlement in blended gas environments was less severe than in pure hydrogen at the same hydrogen partial pressure. However, this inhibiting effect progressively decreased as the hydrogen concentration increased. The authors suggested that natural gas constituents, including CH_4 and heavier hydrocarbons, may reduce hydrogen adsorption and permeation into the steel through competitive surface interactions.[58]

The research leading to these results has received funding from Horizon Europe, the European Union's Framework Programme for Research and Innovation under grant agreement n° 101111888.

3.2.5 Role of H_2S

The literature consistently identifies H_2S as one of the most detrimental gaseous species regarding hydrogen embrittlement of pipeline steels. Previous studies have shown that H_2S significantly increases hydrogen uptake and accelerates hydrogen-assisted cracking and loss of ductility. This behaviour is generally attributed to the dissociative adsorption of H_2S on the steel surface, which promotes the generation and absorption of atomic hydrogen while simultaneously inhibiting hydrogen recombination and desorption. As a result, H_2S-containing environments are widely associated with severe hydrogen-assisted degradation in pipeline steels.[44,59,60]

3.2.6 Role of odorants/THT

Odorization is an essential safety practice in natural gas systems, allowing gas leaks to be easily detected by smell.[61] Odorants are typically added at very low concentrations, usually between 1 and 10 ppm.[62] With the increasing interest in hydrogen transport and hydrogen–natural gas blends, there is growing concern about the possible effect of these compounds on hydrogen embrittlement and hydrogen-assisted degradation of pipeline steels.

According to recent MARCOGAZ data on odorization practices across Europe, sulphur-containing odorants remain the most widely used compounds in gas networks, with tetrahydrothiophene (THT) and tert-butyl mercaptan (TBM)-based mixtures being the dominant odorants in most countries (Figure 12).[63]

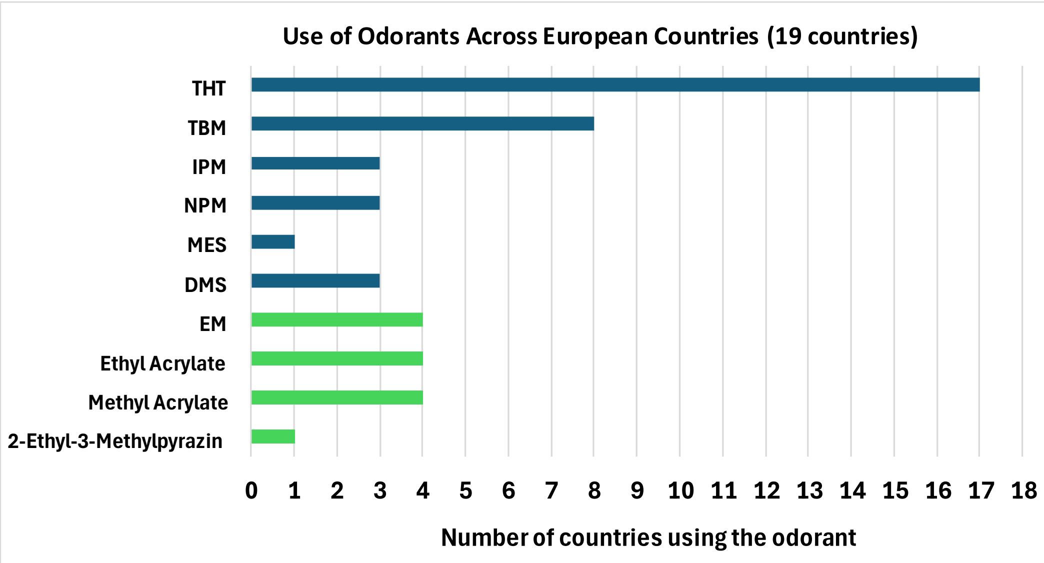

Figure 12 Use of commercial natural gas odorants across 19 European countries. Sulphur-containing odorants are shown in blue and sulphur-free odorants in green. THT = tetrahydrothiophene; TBM = tert-butyl mercaptan; IPM = isopropyl mercaptan; NPM = n-propyl mercaptan; MES = methyl ethyl sulphide; DMS = dimethyl sulphide; EM = ethyl mercaptan.

The influence of odorants on the hydrogen embrittlement in pipelines has not been well studied. Limited studies have examined this issue: Holbrook et al. observed initially promising inhibition effects of methyl mercaptan on fatigue crack growth in hydrogen environments; however, at higher stress intensity ranges, the protective effect diminished. Moreover, they reported, that methyl mercaptan alone might even accelerate crack growth compared to pure hydrogen[50]

Fukuyama et al. found that methyl mercaptan had negligible influence on fatigue crack growth in 4340 steel, but in later work, it significantly promoted hydrogen embrittlement in 2.25Cr-1Mo steel.[45,64]

A recent investigation explored the effect of five different odorants, generally in mixtures, on X42 pipeline steel using SSRT in low-pressure hydrogen environments. The investigated odorants included sulphur-based compounds such as THT, TBM, and DMS, as well as acrylate- and norbornene-based mixtures, at concentrations ranging from approximately 0.05 to 17 ppm in hydrogen. The plastic strain to failure observed

The research leading to these results has received funding from Horizon Europe, the European Union's Framework Programme for Research and Innovation under grant agreement n° 101111888.

in the presence of each candidate gas mixture was comparable to that measured in air, indicating no measurable effect of either the hydrogen or the odorant on the steel under the conditions tested. However, as the study was conducted under relatively low-pressure conditions (7 barg), its direct applicability to high-pressure transmission pipeline systems, where hydrogen embrittlement effects are generally more pronounced, should be considered with caution. [65]

Unpublished results obtained within the ONTZHi project (2023-2025 coordinated by Tecnalia), showed no significant differences between pure hydrogen and hydrogen containing 20 ppm THT in either SSRT or fatigue crack growth testing of API 5L X70 steel at 70 bar gaseous hydrogen. Fracture morphologies also remained broadly similar across environments, suggesting that commercially relevant THT concentrations did not significantly alter hydrogen-assisted degradation behaviour under the investigated conditions (100% hydrogen). [66]

A recent study investigates the effect of mercaptan-based hydrogen odorants on hydrogen uptake in L360NB pipeline steel under high-pressure hydrogen conditions. Using constant load testing and thermal desorption spectroscopy, they found that mercaptan odorants did not significantly increase hydrogen uptake or promote embrittlement, whereas H_2S-containing wet environments showed much higher hydrogen uptake and were identified as more critical for degradation. The study highlights the important distinction between commercial sulphur odorants and reactive sulphur species such as H_2S.[67]

3.2.7 Other

CO and O_2 are frequently discussed in the literature as gaseous inhibitors of hydrogen embrittlement. Although they were not included in the present study since they are not typically present in significant concentrations in natural gas transmission systems, it is interesting to mention that both gases strongly adsorb on iron surfaces and can significantly reduce hydrogen-assisted fatigue crack growth by inhibiting hydrogen adsorption and dissociation at the steel surface. However, the inhibition effectiveness was found to depend strongly on factors such as hydrogen pressure, stress intensity factor and crack growth rate, with the inhibiting effect progressively decreasing under more severe hydrogen embrittlement conditions. [3,50,59]

Based on the literature reviewed above, the effect of gas composition on hydrogen embrittlement appears to depend strongly on gaseous species present, their concentration, material tested and the testing conditions. Therefore, the present work investigates the hydrogen embrittlement behaviour of pipeline steel in three representative gaseous environments designed to simulate realistic European hydrogen–natural gas transmission blends, including both high- and low-calorific gas compositions as well as a blend containing H_2S and THT to assess the influence of reactive sulphur species and commercial sulphur-containing odorants.

3.3 Selection of gas composition for testing within SHIMMER

Three gas mixtures were defined to simulate representative European transmission gas compositions and prepared for the experimental campaign:

1. an **H-gas** mixture
2. an **L-gas** mixture
3. an **H-gas** mixture additionally containing H_2S and THT (H gas + H_2S)

To ensure that the selected compositions are relevant to the gas grid industry in Europe, they were defined together with the industrial partners in SHIMMER and using representative gas-quality data reported by Open Grid Europe (OGE[68]) and the MARCOGAZ LNG quality database indicating the gas composition.[69]

The **H-gas** composition was based on high-calorific natural gas typically characterized by high CH_4 content and low N_2 concentration. Furthermore, it was designed as CO_2-free in order to be representative for Liquefied Natural Gas (LNG).

The research leading to these results has received funding from Horizon Europe, the European Union's Framework Programme for Research and Innovation under grant agreement n° 101111888.

The **L-gas** composition was designed to represent lower-calorific natural gas with lower CH_4 content than H-gas, and higher concentrations o N_2 and CO_2.

The third test environment, contained H_2S close to the limit allowed by the European standards EN16726.[70] H_2S was investigated because of its known influence on hydrogen uptake and hydrogen-assisted degradation, while THT was included as a representative sulphur-containing odorant used in natural gas distribution networks. This scenario was selected to assess the synergistic effect of H_2S in accelerating hydrogen embrittlement when blended with hydrogen.

A hydrogen concentration of 20 vol% was selected for all blended environments, since this level is commonly considered among the upper hydrogen blending ranges currently discussed for hydrogen injection into existing natural gas transmission infrastructure.

The certified detailed gas compositions are summarized in Table 5.

Table 5 The certified compositions for the gas blend mixtures utilised for testing. Gas composition is expressed in vol.% for all components except H_2S and THT, which are reported in ppm.

Gas component	H gas	L gas	H gas + H_2S
Methane	Balance	Balance	Balance
Nitrogen	0.05 %	11.15 %	0.05 %
Carbon dioxide	0.00 %	1.00%	0.00 %
Ethane	0.29 %	2.98%	0.28 %
Propane	0.18 %	0.85 %	0.18 %
Hydrogen	20.00 %	19.95 %	20.1 %
H_2S			4.76 ppm
Odorant (THT)			22.8 ppm

As a reference media, 100% hydrogen tests, grade 5.6 hydrogen (>99.9996%) was used; purity tolerances are detailed in **Table 6**.

Table 6 Certified composition for the grade 5.6 H_2 gas (NIPPON GASES).

Grade	H2 (%)	CO + CO2 (ppm)	Hydrocarbons (ppm)	N2 (ppm)	O2 (ppm)	H2O (ppm)
5.6	**99.9996**	**<0.2**	**<0.1**	**<2**	**<0.5**	**<2**

3.4 Material

API 5L X70 steel was selected for this study because previous inventory and infrastructure assessments performed within the SHIMMER project identified X70 as one of the most widely used grades in the existing natural gas transmission network. In addition, its relatively high strength suggests an increased susceptibility to hydrogen embrittlement compared to lower-strength pipeline steels. The chemical composition is summarized in Table 7.

The research leading to these results has received funding from Horizon Europe, the European Union's Framework Programme for Research and Innovation under grant agreement n° 101111888.

Table 7 Certified chemical composition of the X70 steel (wt. %).

C	Mn	Si	P	S	Cr	Ni	Mo	Cu	Ti
0.13	1.65	0.26	0.018	<0.010	0.021	0.015	0.038	0.016	0.012

Steel samples were obtained from a vintage pipeline of grade X70 (API 5L) used in the natural gas transmission network with a nominal outer diameter and thickness of 406 mm and 8.2 mm respectively, a yield stress of 549 MPa, a tensile strength of 675 MPa and a ferrite/bainite microstructure (Figure 13).

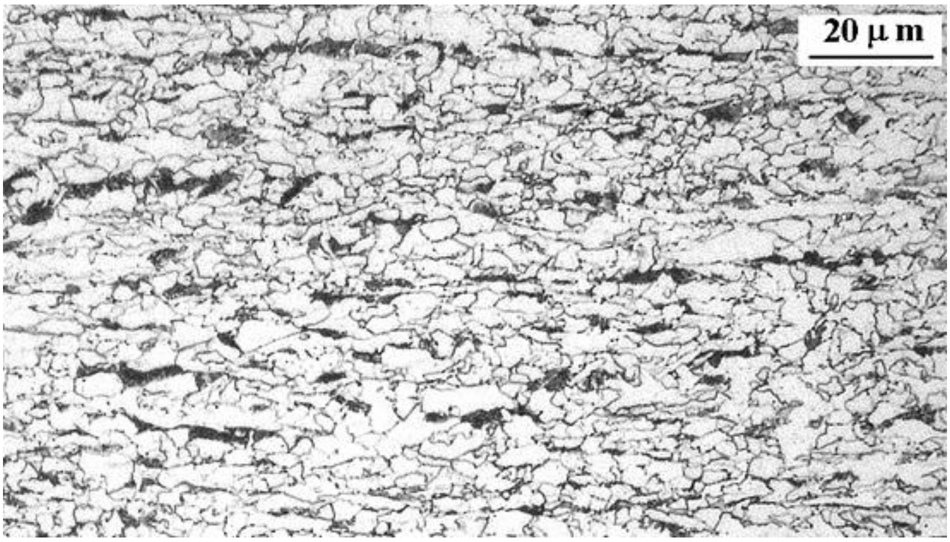

Figure 13 Image of the microstructure for the tested API 5L X70 steel.

3.5 Methods

Hydrogen embrittlement susceptibility was evaluated by means of Slow Strain Rate Testing (SSRT) testing under high-pressure gaseous environments. The experimental methodology was based on the following standards:

- **ANSI/CSA CHMC 1-2014 (R2018)**: Test methods for evaluating material compatibility in compressed hydrogen applications. [71]
- **ASTM G129-21:** Standard Practice for Slow Strain Rate Testing to Evaluate the Susceptibility of Metallic Materials to Environmentally Assisted Cracking.[72]
- **ASTM G142-98:** Standard Test Method for Determination of Susceptibility of Metals to Embrittlement in Hydrogen Containing Environments at High Pressure, High Temperature, or Both.[73]

3.5.1 Test specimens

Specimens were machined in the longitudinal direction, centred within the pipe thickness. Figure 14 shows a diagram with the nominal dimensions of the specimens used for testing. These were cylindrical "hourglass" type specimens with a minimum diameter of 4 mm, a gauge length of 28 mm and a curvature radius of 50 mm.

The research leading to these results has received funding from Horizon Europe, the European Union's Framework Programme for Research and Innovation under grant agreement n° 101111888.

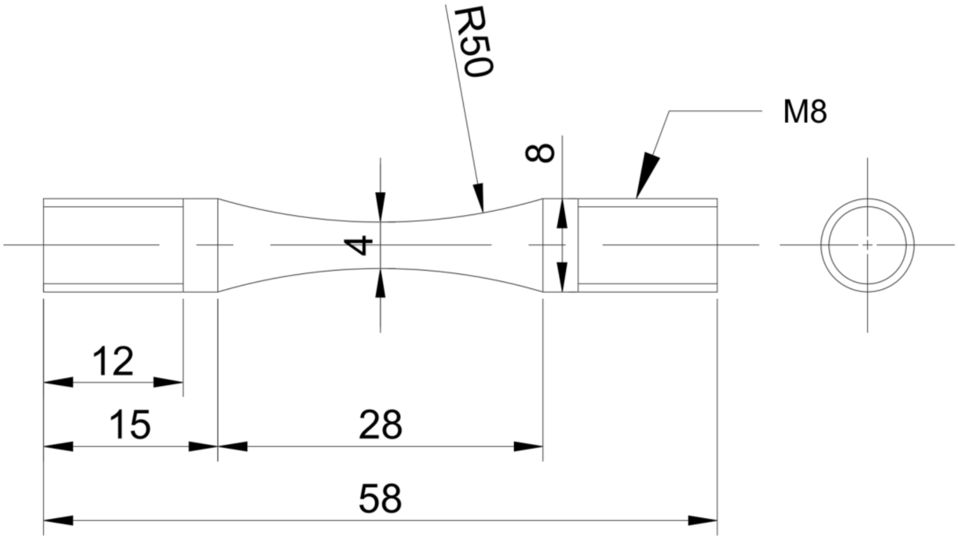

Figure 14 Diagram of the "hourglass" type specimens used for SSRT testing (dimensions in mm).

Although the specimen geometry differs from the standard smooth tensile geometry described in ASTM G142, the standard explicitly permits alternative geometries when imposed by material or testing constraints, provided that comparisons are performed only between similar specimens. In this study all environments investigated were evaluated using identical specimen geometry and testing conditions, allowing direct comparison of the results.

3.5.2 Test matrix and experimental methods

The test matrix is shown in Table 8. Eleven specimens were tested in total: three specimens for each investigated gas composition, and two additional specimens tested in pure hydrogen (100% H_2), which were used as a reference environment representing the maximum degree of hydrogen embrittlement experienced by the X70 material. The testing pressure was selected as 80 barg to reproduce representative operating pressures commonly encountered in transmission networks.

Table 8 Test matrix for SSRT testing

Material	Test Environment	Pressure (barg)	Number of Tests	Crosshead displacement rate (mm/s)
X70	**H_2** (100%, reference)	80	2	2,8×10^{-5}
	H gas (20% of H_2)	80	3	
	L gas (20% of H_2)	80	3	
	H gas + H_2S (20% of H_2)	80	3	

SSRT tests were carried out on a CORTEST testing machine (Figure 15) at a crosshead displacement rate of 2.8×10^{-5} mm/s. A strict protocol was followed to maintain gas purity inside the autoclave. Specimens were cleaned with acetone and ethanol and air-dried before loading. After loading the specimens, the autoclave was sealed and purged ten times with nitrogen (10 bar) to eliminate air, O_2, and moisture. A helium leak test was then performed by pressurizing the vessel to the test pressure and monitoring stability for 15 minutes. After evacuating the helium, the system underwent ten purges with the test gas (up to 10 bar). Finally, the autoclave was pressurized with the test gas to a pressure of 80 bar. All tests were performed at room temperature (17-

The research leading to these results has received funding from Horizon Europe, the European Union's Framework Programme for Research and Innovation under grant agreement n° 101111888.

23°C), with a 10-minute stabilization period after pressurization, before commencing the loading at the desired crosshead displacement rate. The specimens were loaded to failure.

Figure 15 Test machine for SSRT, fracture toughness, and fatigue testing in compressed hydrogen.

Post-failure, the fractured samples were analysed via optical microscopy and scanning electron microscopy (SEM) to measure the final diameters at the necking zone and characterize the morphology of the fracture surface.

3.5.3 Analysis

Once the tests are completed, the load, displacement, and specimen diameter measurements (initial and final) can be used to generate the stress vs. plastic strain curves, and to estimate the values of interest for evaluating the degree of embrittlement. Three primary parameters are used to compare the degree of hydrogen embrittlement: ultimate tensile strength, plastic strain to failure and reduction of area.

3.5.3.1 Ultimate tensile strength (MPa)

The equation used to estimate the ultimate tensile stress (engineering stress), σ_{uts}, is:

$$\boldsymbol{\sigma_{uts} = \frac{F_{max}}{A_i}},$$ **Equation 5**

where F_{max} is the maximum load recorded during the tensile test and A_i is the minimum initial cross-sectional area of the specimen at the start of the test:

$$\boldsymbol{A_i = \frac{\pi D_i^2}{4}},$$ **Equation 6**

The research leading to these results has received funding from Horizon Europe, the European Union's Framework Programme for Research and Innovation under grant agreement n° 101111888.

where D_i is the initial diameter of the specimen.

3.5.3.2 Plastic strain

The plastic strain is determined by first calculating the total engineering strain (ε_{total}), which is defined as the ratio of the change in length (displacement, ΔL) to the original gauge length (L_0):

$$\boldsymbol{\varepsilon_{total} = \frac{\Delta L}{L_0}}$$ **Equation 7**

In this experimental setup, since displacement is measured via external LVDTs, the crosshead displacement provided by the machine is considered an overestimate of the actual displacement of the tensile sample within the autoclave. Consequently, to obtain the true deformation experienced by the specimen, the plastic strain (ε_{pl}) is calculated by subtracting the elastic component of the deformation (ε_{el}) from the total measured strain:

$$\boldsymbol{\varepsilon_{pl} = \varepsilon_{total} - \varepsilon_{el}}$$ **Equation 8**

The elastic component is determined by multiplying the applied force (F) by the inverse of the gradient of the linear-elastic region of the force-displacement curve (the compliance during the elastic region, C):

$$\boldsymbol{\varepsilon_{el} = F \cdot C}$$ **Equation 9**

By utilizing the slope of the elastic region, the elastic component (including both the sample and the machine load-train compliance) is isolated and removed, ensuring that the resulting value represents only the plastic deformation component of the specimen.

3.5.3.3 Reduction of area

The reduction of area at the neck region, RA, is calculated as

$$\boldsymbol{RA\ (\%) = \frac{A_i - A_f}{A_i} \,.\, 100}$$ **Equation 10**

where A_i and A_f are the initial and final areas in the necking zone, respectively. To calculate the final area A_f, two perpendicular diameters (d_1 and d_2) must be measured at the neck:

$$\boldsymbol{A_f = \frac{\pi \cdot d_1 \cdot d_2}{4}}$$ **Equation 11**

3.6 Results and discussion

3.6.1 SSRT results

The mechanical response of the X70 steel under the different environments is illustrated through the engineering stress vs. plastic strain curves in Figure 16 and summarized in Table 9.

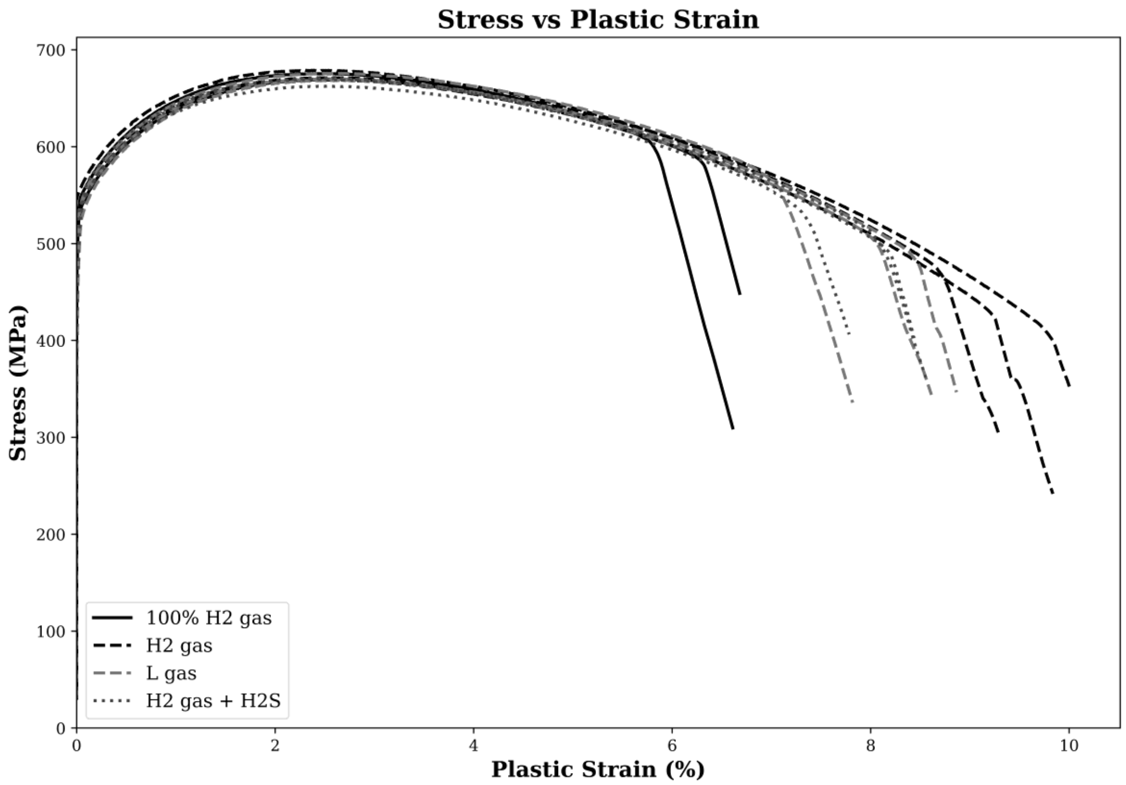

Figure 16 Engineering stress vs. plastic strain curves for the SSRT tests in different environments

It can be seen in Figure 16 that the stress-strain curves for all specimens exhibit a similar profile, with the σ_{uts} remaining relatively constant regardless of the gas composition. The mean σ_{uts} values ranged from 667.7 MPa for the **H-gas+H$_2$S** blend to 673.1 MPa for the **H-gas** blend. This indicates that the hydrogen containing environments, at the tested pressure and strain rate, do not significantly alter the tensile strength of the X70 steel. While the strength remained stable, a significant variation was observed in the ductility parameters (ε_{pl} and RA), which are the primary indicators of hydrogen embrittlement.

To evaluate the degree of hydrogen embrittlement the reduction of area (RA, Figure 17), the plastic strain to failure (ε_{pl} Figure 18), and the ultimate tensile strength (σ_{uts} Figure 19) were compared across the four tested environments.

The specimens tested in 100% H_2 exhibited the lowest ductility, with a mean RA of 47.4% and a mean plastic strain to failure of 6.65%. As expected, this environment represents the maximum degree of embrittlement, serving as the baseline for assessing the influence of the natural gas blends. Compared with the 100% H_2 environment, all 20% H_2 gas mixtures exhibited substantially reduced hydrogen-induced ductility loss. The **H-gas** blend showed the lowest hydrogen embrittlement susceptibility, with a mean RA of 71.3% and a plastic strain of 9.72%. In contrast, the **L-gas** blend showed slightly higher hydrogen embrittlement susceptibility compared with the **H-gas** blend, with a mean RA of 61.0% and a plastic strain of 8.43%. Since both blends contained the same nominal H_2 concentration, the observed difference is likely related to the different gas

The research leading to these results has received funding from Horizon Europe, the European Union's Framework Programme for Research and Innovation under grant agreement n° 101111888.

matrix composition of the **L-gas** blend, particularly its lower CH_4 content and higher concentrations of N_2, CO_2 and C_2–C_3 hydrocarbons.

The addition of H_2S to the **H-gas** blend led to a slight increase in hydrogen embrittlement susceptibility compared to H_2S free **H-gas**. The mean RA decreased to 59.8% and the plastic strain to 8.26%. Although the effect was relatively moderate, the trend is consistent with the known role of **H_2S** in promoting hydrogen uptake and hydrogen-assisted degradation in steels.

Table 9 Main SSRT results for the different gas compositions.

Specimen ID	Environment	RA (%)	σ_{uts} (MPa)	ε_{pl} (%)
X70_SSRT_14_H2_gas	**H_2 (100%)**	49,2	675,6	6,68
X70_SSRT_15_H2_gas		45,6	669,7	6,61
Mean		**47,4**	**672,6**	**6,65**
X70_SSRT_3_blend_H_gas	**H gas (blend)**	75,6	671,2	10,01
X70_SSRT_4_blend_H_gas		66,0	678,9	9,30
X70_SSRT_5_blend_H_gas		72,2	669,3	9,84
Mean		**71,3**	**673,1**	**9,72**
X70_SSRT_6_blend_L_gas	**L gas (blend)**	62,2	670,2	8,61
X70_SSRT_7_blend_L_gas		64,5	669,0	8,87
X70_SSRT_8_blend_L_gas		56,3	675,8	7,82
Mean		**61,0**	**671,7**	**8,43**
X70_SSRT_9_blend_H2S_gas	**H gas + H_2S (blend)**	56,9	662,4	7,78
X70_SSRT_10_blend_H2S_gas		60,7	670,8	8,57
X70_SSRT_11_blend_H2S_gas		61,8	669,8	8,44
Mean		**59,8**	**667,7**	**8,26**

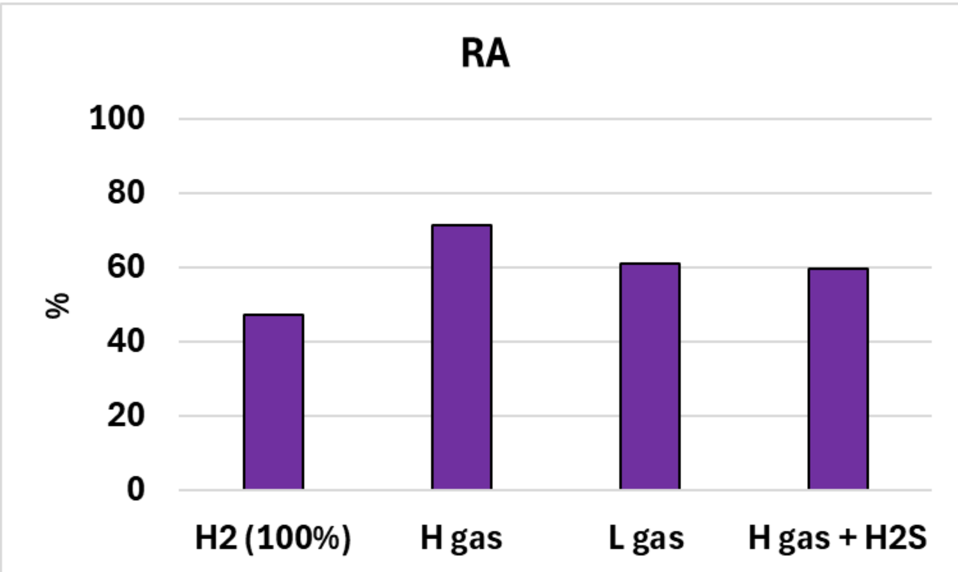

Figure 17 Comparison of RA for X70 specimens tested under four different hydrogen containing atmospheres. Bars indicate the mean value for each environment

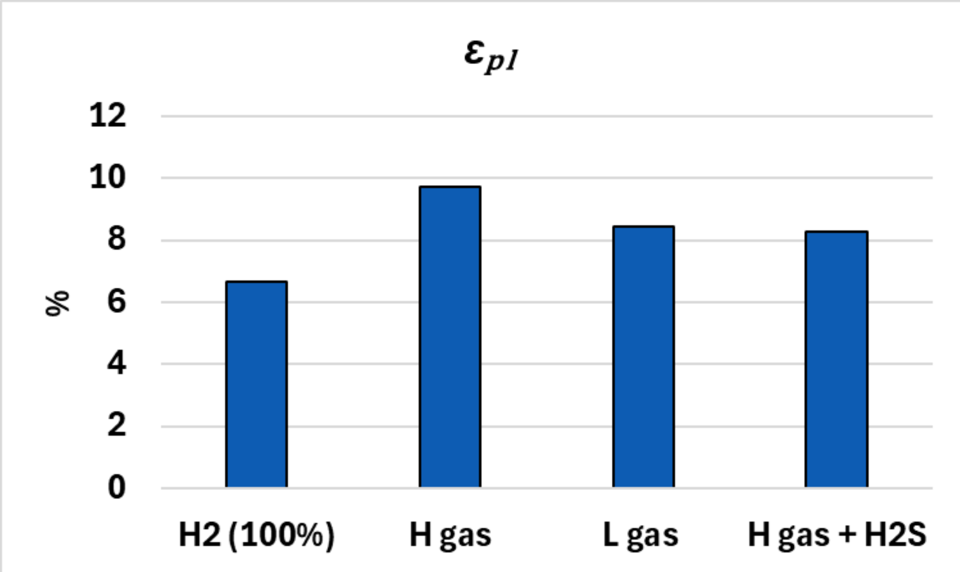

Figure 18 Comparison of ε_{pl} for X70 specimens tested under four different hydrogen containing atmospheres. Bars indicate the mean value for each environment.

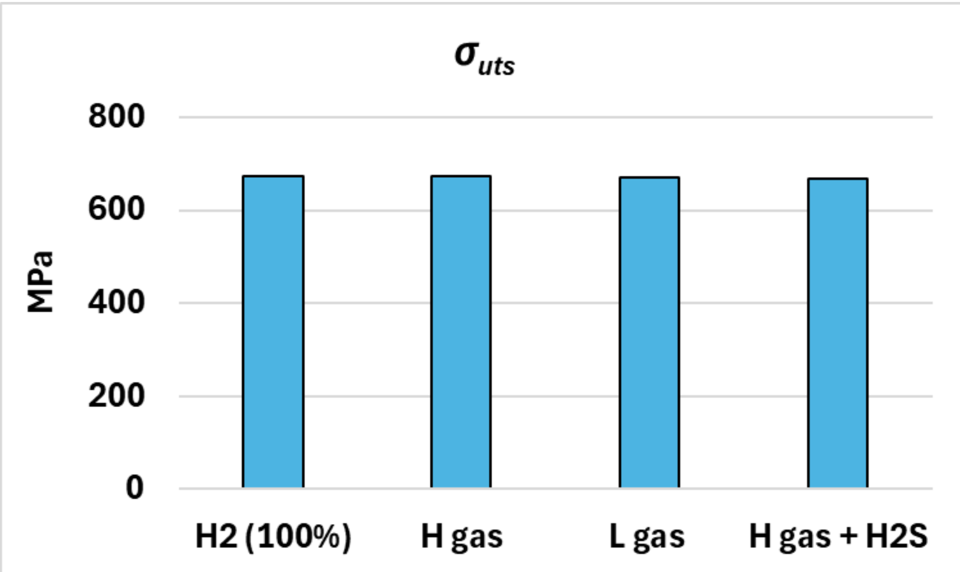

Figure 19 Comparison of σ_{uts} for X70 specimens tested under four different hydrogen containing atmospheres. Bars indicate the mean value for each environment

3.6.2 Post-mortem fracture analysis

To complement the mechanical data, the fracture surfaces of representative specimens from each environment were analysed using SEM. This allows for the correlation between the macroscopic ductility loss and the microscopic failure mechanisms. The specimen tested in the **H-gas** blend exhibited the most ductile behaviour, characterized macroscopically by a classic "cup and cone" fracture morphology (Figure 21a). High-magnification SEM images of the centre region (Figure 21b) reveal large, deep dimples, which are indicative of ductile tearing through microvoid coalescence. At the periphery (Figure 21c), the rupture is characterized by finer microvoid coalescence and the presence of shear lips. Notably, no significant secondary cracking was

The research leading to these results has received funding from Horizon Europe, the European Union's Framework Programme for Research and Innovation under grant agreement n° 101111888.

observed, confirming that this environment provides the highest resistance to hydrogen embrittlement among the tested scenarios.

Specimens tested in the **L-gas** and **H-gas+H_2S** blends also exhibited ductile characteristics at high magnification (x1000), with fine dimples evidencing microvoid coalescence (Figure 22b,c and Figure 23b,c). However, a distinct difference was observed compared to the **H-gas** blend: the dimples at the centre were similar in size to those at the periphery and significantly smaller than those found in the **H-gas** specimen centre. This suggests a more localized plasticity and a generally more fragile macroscopic fracture. Furthermore, the fracture surfaces for both blends deviated from the cup-and-cone morphology, instead showing prominent secondary cracks running on a plane normal to the radial direction of the pipe. These secondary cracks are clear indicators of an increased level of embrittlement.

The most severe embrittlement was observed in the pure H_2 environment (Figure 20). The periphery of the fracture surface showed clear evidence of cleavage-type fracture, characterized by flat facets that indicate fragile crack initiation and propagation from the specimen surfaces. In contrast, the centre of the sample displayed fine dimples associated with ductile tearing. This suggests a mixed-mode failure mechanism: hydrogen embrittlement triggered fragile cracking at the periphery, which propagated until the remaining cross-sectional area at the neck became insufficient to support the load, eventually leading to ductile overload. Similar to the **L-gas** and **H-gas+H_2S** blends, prominent secondary cracks perpendicular to the radial direction of the pipe were present, further confirming the high susceptibility of the X70 material to embrittlement in pure hydrogen.

These SEM observations correlate well with the mechanical data obtained from the SSRT tests. The high degree of ductility observed in the **H-gas** blend, characterized by large dimples and an absence of secondary cracks, is consistent with its high RA and ε_{pl} values. For the **L-gas** and **H-gas+H_2S** blends, the appearance of smaller dimples and prominent secondary cracks aligns with the moderate reduction in ductility, suggesting a shift toward more localized plasticity. Most severely, the presence of clear cleavage facets and secondary cracking in the pure H_2 environment correlates with the lowest RA and ε_{pl} values recorded, confirming that pure hydrogen induces the most significant susceptibility to brittle fracture.

The research leading to these results has received funding from Horizon Europe, the European Union's Framework Programme for Research and Innovation under grant agreement n° 101111888.

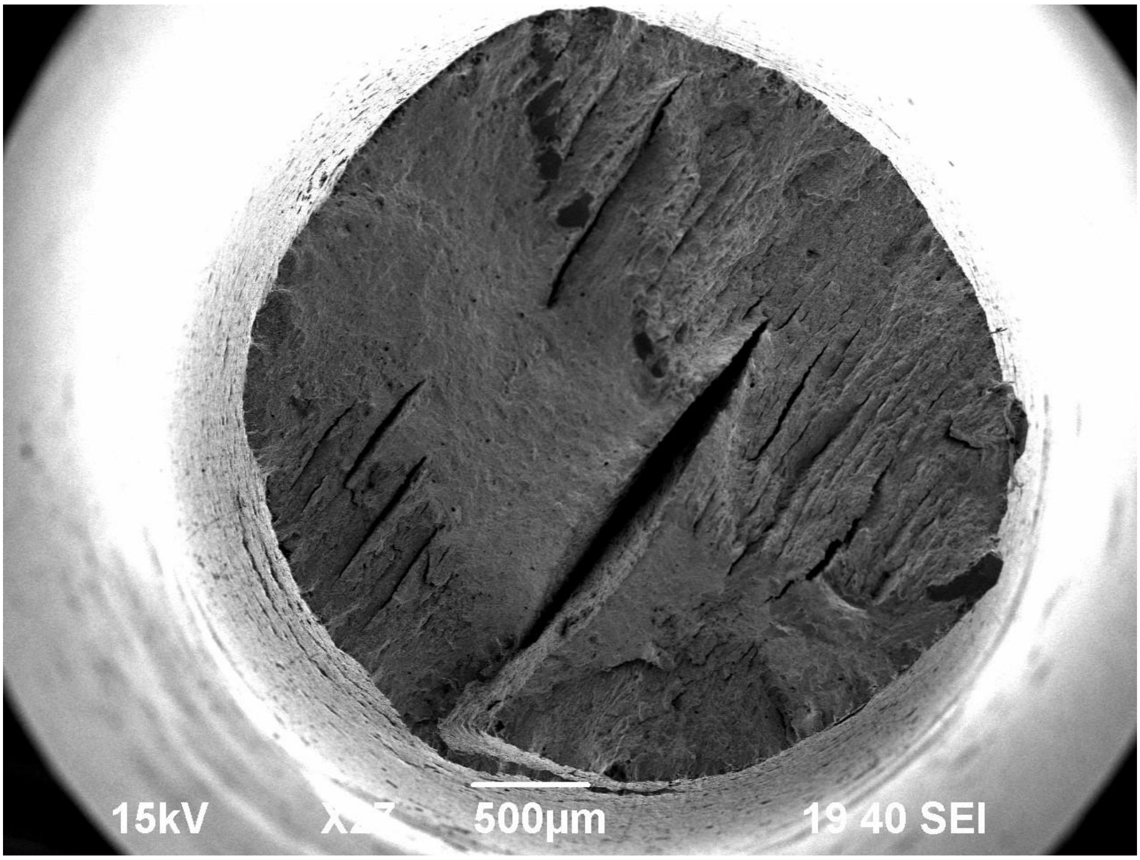

(a) Full fracture surface

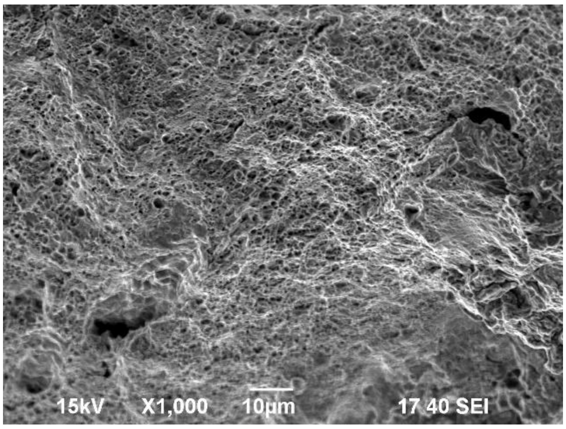

(b) Centre – x1000 - Ductile

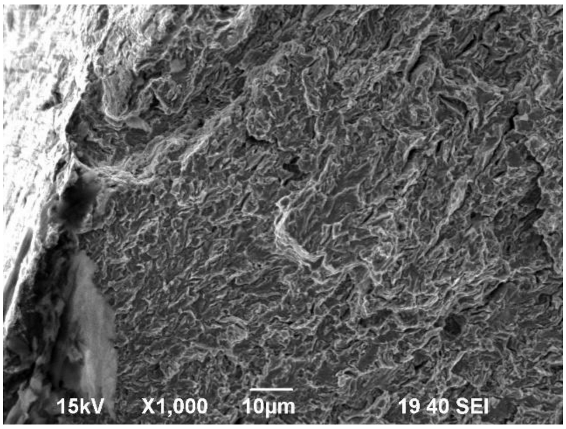

(c) Periphery – x1000 - Cleavage

Figure 20 Fracture surface for one of the samples tested in pure hydrogen.

The research leading to these results has received funding from Horizon Europe, the European Union's Framework Programme for Research and Innovation under grant agreement n° 101111888.

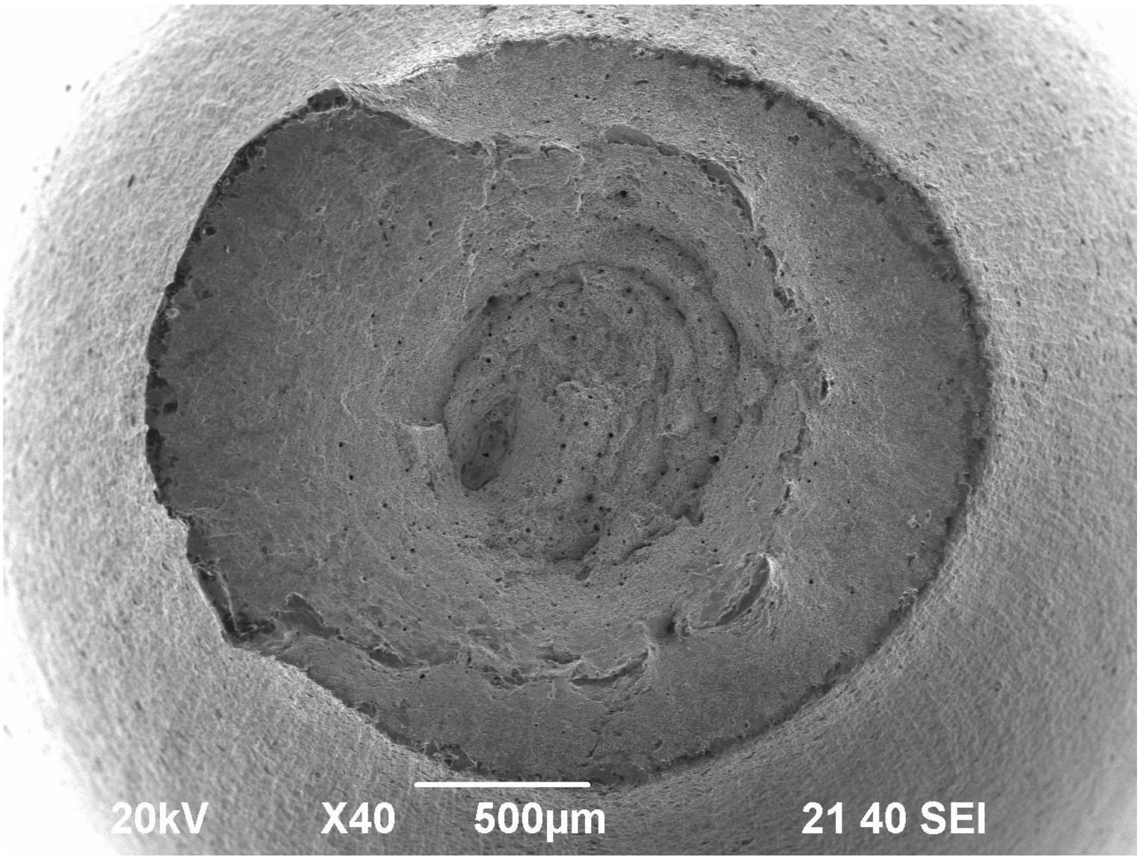

(a) Full fracture surface – Cup and cone (ductile)

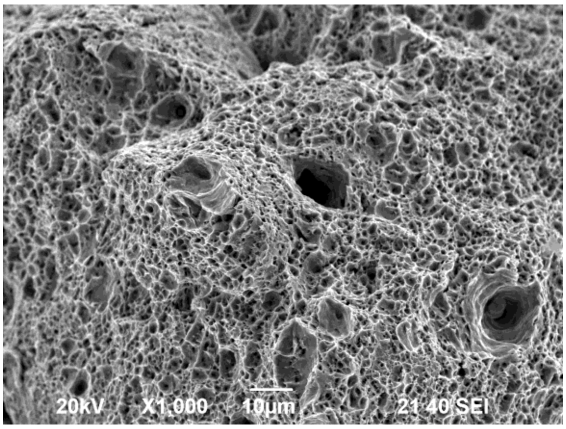

(b) Centre – x1000 - Ductile

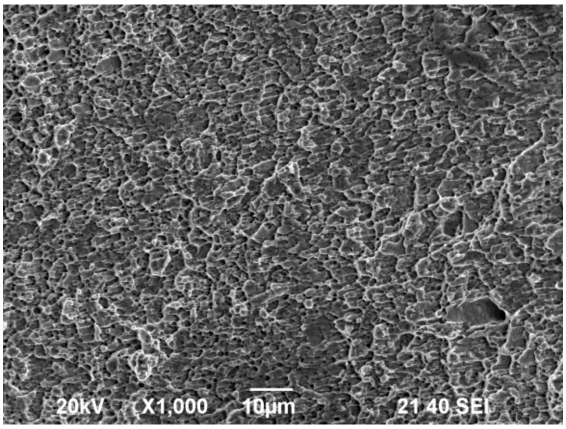

(c) Periphery – x1000 - Ductile

Figure 21 Fracture surface for one of the samples tested in H-gas blend.

The research leading to these results has received funding from Horizon Europe, the European Union's Framework Programme for Research and Innovation under grant agreement n° 101111888.

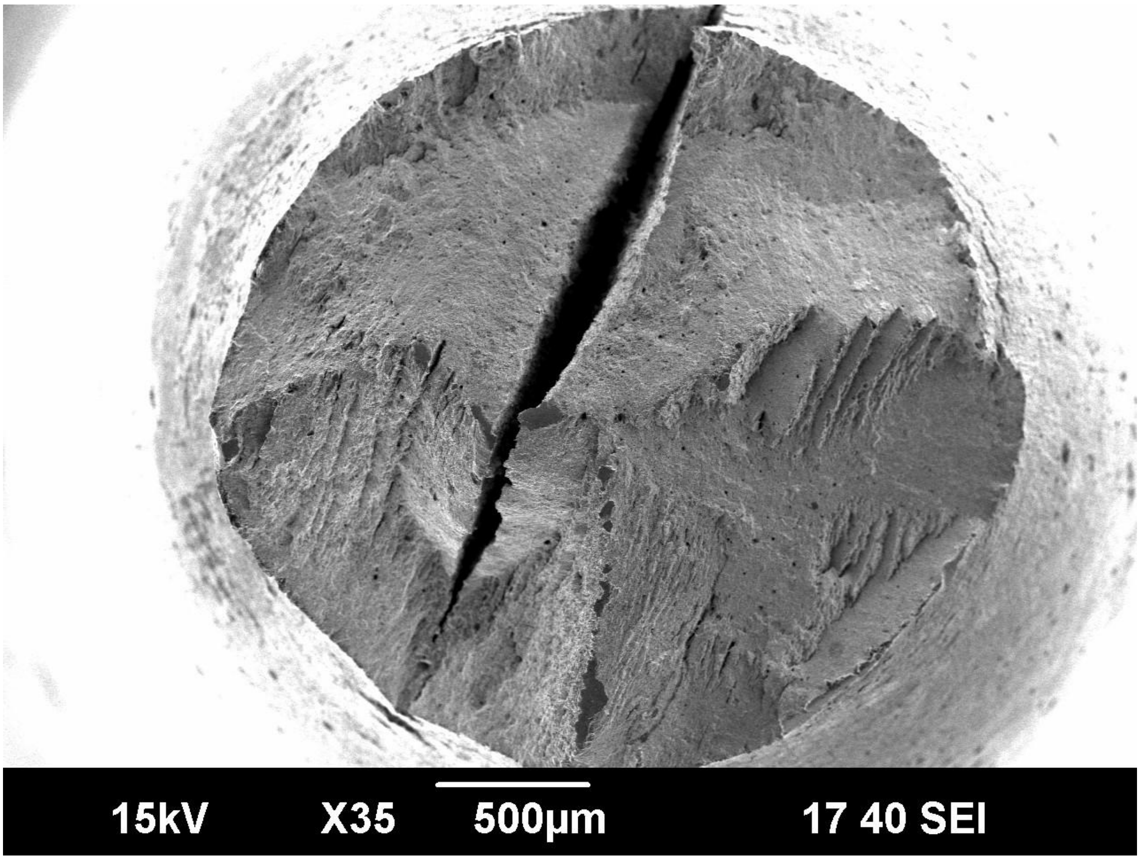

(a) Full fracture surface

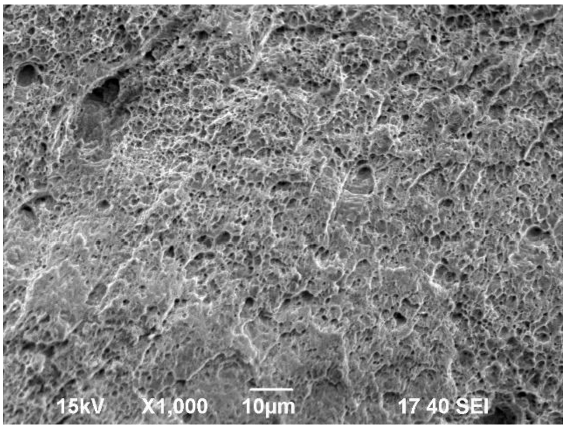

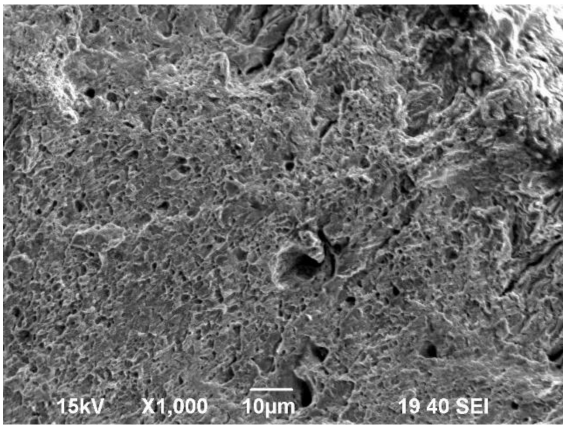

(b) Centre – x1000 - Ductile

(c) Periphery – x1000 - Ductile

Figure 22 Fracture surface for one of the samples tested in L-gas blend.

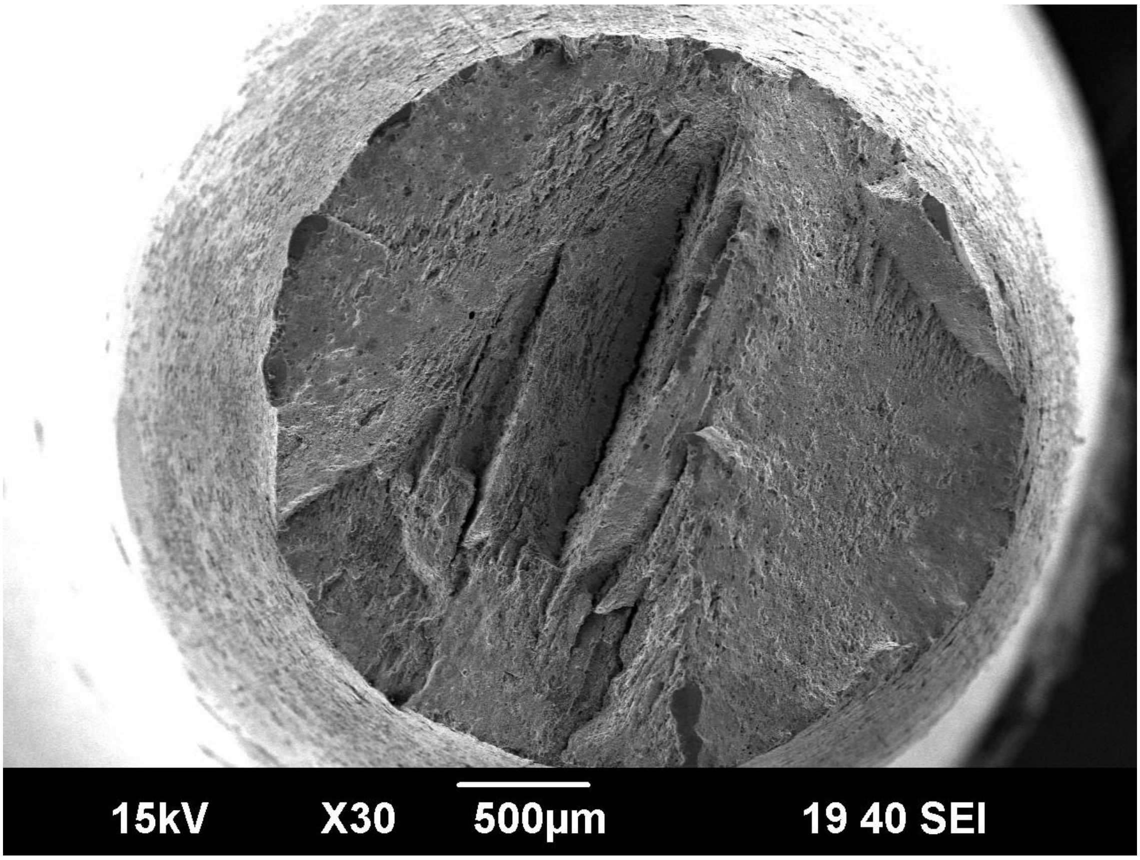

(a) Full fracture surface

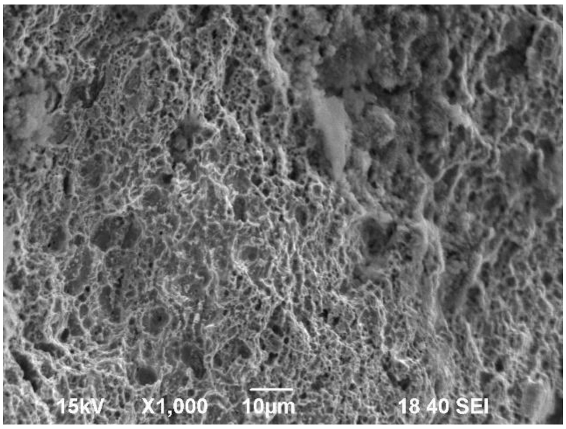

(b) Centre – x1000 - Ductile

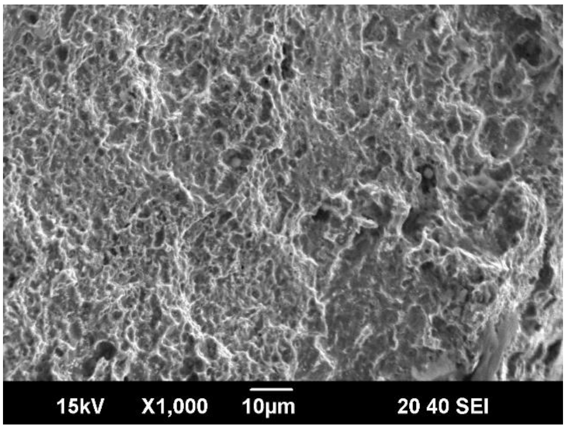

(c) Periphery – x1000 - Ductile

Figure 23 Fracture surface for one of the samples tested in H-gas + H_2S blend.

The research leading to these results has received funding from Horizon Europe, the European Union's Framework Programme for Research and Innovation under grant agreement n° 101111888.

3.6.3 Discussion

The results show that hydrogen mainly affected ductility-related properties, whereas the ultimate tensile strength remained essentially unchanged. This behaviour is consistent with previous studies on pipeline steels of similar grades, which reported significant reduction in elongation and RA, but only minor changes in tensile strength under hydrogen-containing environments.[74]

The degree of embrittlement, in order of increasing severity, follows the trend:

H-gas blend → **L-gas** blend → **H-gas+**H_2S blend → Pure **H2**

The **H-gas** blend exhibited the lowest hydrogen embrittlement susceptibility among the investigated blended environments, showing the highest reduction of area and plastic strain values. This behaviour is likely related to the high CH_4 content of the blend together with the absence of additional potentially reactive gaseous species. As discussed in the literature, CH_4 may exert a weak competitive adsorption effect on the steel surface, partially reducing hydrogen adsorption and hydrogen ingress into the material. Although the exact mechanism cannot be confirmed from the present results alone, the observed behaviour is consistent with previous studies reporting a mild inhibitory effect of CH_4-containing natural gas blends on hydrogen-assisted degradation.

The **L-gas** blend showed slightly higher hydrogen embrittlement susceptibility than the **H-gas** blend, as indicated by the lower reduction of area and plastic strain values. Compared with the **H-gas** environment, the **L-gas** mixture contained lower CH_4 concentrations together with 10% N_2, 1% CO_2, some ethane and propane. However, based on the available literature, the more pronounced degradation may be associated with the reduced inhibitory effect of CH_4 together with a possible contribution of CO_2 to hydrogen-assisted degradation. Although the role of CO_2 remains controversial in the literature, several studies have reported that low CO_2 concentrations can facilitate hydrogen uptake and crack growth under certain gaseous hydrogen conditions, which is consistent with the present observations.

The **H-gas +** H_2S blend exhibited the lowest ductility among the investigated blends. When compared with the **H-gas** environment, which was otherwise compositionally similar, the observed difference may be associated with the presence of ppm-level H_2S. Tetrahydrothiophene (THT) was also present in this blend; however, based on the available literature and previous experimental observations at Tecnalia, THT is generally expected to have little or no significant influence on hydrogen-assisted degradation. Nevertheless, its effect within the specific gas mixture investigated in this study cannot be completely excluded without dedicated experimental verification.

Despite the lower ductility observed in the **H-gas +** H_2S environment, its overall behaviour remained comparable to that of the **L-gas** mixture, which did not contain H_2S or odorant. This suggests that sulphur-containing additives present at concentrations within the limits permitted by gas quality specifications do not appear to induce severe additional degradation. Instead, their effect remains within the range of variations associated with other sulphur-free gaseous components commonly encountered in natural gas compositions. Furthermore, the results indicate that the influence of complex gas mixtures cannot be interpreted solely as the sum of the effects of individual components, highlighting the importance of mixture-specific interactions.

3.7 Conclusion

The literature review showed that hydrogen embrittlement in hydrogen-containing natural gas systems composed of multiple gas components cannot be predicted solely from hydrogen partial pressure or from the individual presence of specific gaseous species. Instead, the observed degradation indicates a complex and non-linear interaction between gas composition, impurity concentration, competitive adsorption process, hydrogen transport kinetics and testing conditions. Previous studies have shown that the behaviour of multicomponent gas mixtures cannot be interpreted as the simple sum of the effects of individual gas components. Interactions between gaseous species appear to modify the overall hydrogen-assisted degradation response, resulting in complex and potentially non-linear behaviour.

The present results support this complexity. The methane-rich **H-gas** blend exhibited lower embrittlement susceptibility than environments containing less CH_4 and additional CO_2 and trace H_2S. However, the observed differences cannot be unambiguously attributed to a single gaseous component. For example, the slightly higher degradation observed in the simulated **L-gas** environment may be associated with both the lower CH_4 concentration and the presence of CO_2. Similarly, although the **H-gas + H_2S** blend showed slightly lower ductility than the **H-gas** environment, the overall behaviour remained comparable to the **L-gas** blend despite the presence of trace H_2S. These observations further highlight the difficulty of isolating the individual contribution of specific gas species in realistic multicomponent transmission gas mixtures.

From an application perspective, several observations are relevant: First, the methane-rich **H-gas** blend exhibited the lowest embrittlement susceptibility among the investigated gas mixtures, suggesting that high-CH_4 transmission gases may be less aggressive. This is particularly relevant since **H-gas** currently represents by far the predominant transmission gas quality across European gas networks. Moreover, the simulated **H-gas** environment was also representative of LNG-derived gas streams due to the absence of CO_2, which is typically removed during LNG processing. Finally, although the **H-gas + H_2S** blend showed slightly higher embrittlement than the **H-gas** environment, the overall degree of degradation remained comparable to that of the **L-gas** blend which is H_2S-free. This suggests that ppm-level H_2S and THT under the investigated conditions did not produce a disproportionately severe additional embrittlement effect.

The research leading to these results has received funding from Horizon Europe, the European Union's Framework Programme for Research and Innovation under grant agreement n° 101111888.

4 Overall conclusions and implications for hydrogen repurposing

This deliverable builds on the material and component compatibility screening performed in D3.1 and provides a more detailed assessment of two specific aspects relevant to hydrogen-natural gas blends: structural integrity and defect tolerance of repurposed pipelines, and the influence of gas quality on hydrogen embrittlement behaviour in pipeline steel. The assessment shows that hydrogen repurposing cannot be judged from hydrogen concentration or operating pressure alone. Under the conservative assumptions adopted, hydrogen-containing service reduces the calculated fatigue-life margin and can reduce the tolerance to critical crack-like defects. The governing response depends on the combined influence of pressure, pipeline geometry, material grade, fracture toughness, residual stresses, fatigue crack growth behaviour and inspection capability.

From the structural integrity assessment, hydrogen-containing service was shown to reduce integrity margins by accelerating fatigue crack growth and lowering fracture toughness. The fatigue-life and detectability screening maps provide a conservative basis for identifying pipeline configurations requiring detailed engineering critical assessment, refined material data, pressure-history analysis or improved inspection capability.

Overall, the assessment provides a structured basis for ranking repurposing scenarios and identifying where additional integrity work is required. It does not establish universal hydrogen blending limits or provide final acceptance decisions for individual pipelines. A favourable screening result indicates a lower relative concern under the adopted assumptions, whereas an unfavourable result identifies the need for additional evidence or mitigation before hydrogen-containing service is considered.

From the gas-quality and gas composition assessment, among the tested 20% hydrogen blends, the methane-rich **H-gas** mixture exhibited the lowest embrittlement susceptibility, whereas the **L-gas** and **H-gas + H_2S** mixtures showed slightly higher degradation. The **H-gas + H_2S** blend showed lower ductility than the **H-gas** blend, but its overall behaviour remained comparable to the H_2S-free L-gas mixture. This indicates that ppm-level H_2S and THT did not produce a disproportionately severe additional embrittlement effect under the conditions investigated. The literature review and the results both highlight that the behaviour of complex multicomponent gas mixtures remains difficult to predict from the effect of individual gas species alone or hydrogen partial pressure. Important knowledge gaps remain regarding gas-species interactions and their influence on hydrogen-assisted degradation under realistic gas-grid conditions.

Overall, the findings support a case-specific approach to hydrogen repurposing, combining structural integrity assessment, inspection planning, material compatibility evaluation and realistic gas-composition considerations. The results should be interpreted as conservative screening and decision-support guidance rather than universal acceptance criteria or general blending limits.

The research leading to these results has received funding from Horizon Europe, the European Union's Framework Programme for Research and Innovation under grant agreement n° 101111888.

5 References

[1] P.E. Dodds, S. Demoullin, Conversion of the UK gas system to transport hydrogen, Int. J. Hydrogen Energy 38 (2013) 7189–7200. https://doi.org/10.1016/j.ijhydene.2013.03.070.

[2] M.W. Melaina, O. Antonia, M. Penev, Blending Hydrogen into Natural Gas Pipeline Networks: A Review of Key Issues, 2013. http://www.osti.gov/bridge.

[3] C. San Marchi, B.P. Somerday, Technical Reference On Hydrogen Compatibility Of Materials, Sand2008-1163 (2012) 292. http://energy.sandia.gov/wp/wp-content/gallery/uploads/SAND2012_7321.pdf.

[4] J.A. Ronevich, E.J. Song, B.P. Somerday, C.W. San Marchi, Hydrogen-assisted fracture resistance of pipeline welds in gaseous hydrogen, Int. J. Hydrogen Energy 46 (2021) 7601–7614. https://doi.org/10.1016/j.ijhydene.2020.11.239.

[5] C. San Marchi, B.P. Somerday, K.A. Nibur, D.G. Stalheim, T. Boggess, S. Jansto, Fracture Resistance and Fatigue Crack Growth of X80 Pipeline Steel in Gaseous Hydrogen, in: Volume 6: Materials and Fabrication, Parts A and B, ASMEDC, 2011: pp. 841–849. https://doi.org/10.1115/PVP2011-57684.

[6] N. Nanninga, A. Slifka, Y. Levy, C. White, A review of fatigue crack growth for pipeline steels exposed to hydrogen, J. Res. Natl. Inst. Stand. Technol. 115 (2010) 437. https://doi.org/10.6028/jres.115.030.

[7] H. Wang, N.O. Larrosa, D. Engelberg, R. Best, L. Susmel, A Statistical Review of Hydrogen Effects on the Fatigue and Fracture Behavior of Steel, Fatigue Fract. Eng. Mater. Struct. 48 (2025) 3613–3644. https://doi.org/10.1111/ffe.14687.

[8] M.F.W. Chowdhury, C. V. Tapia-Bastidas, J. Hoschke, J. Venezuela, A. Atrens, A review of influence of hydrogen on fracture toughness and mechanical properties of gas transmission pipeline steels, Int. J. Hydrogen Energy 102 (2025) 181–221. https://doi.org/10.1016/j.ijhydene.2025.01.018.

[9] I.M. Robertson, P. Sofronis, A. Nagao, M.L. Martin, S. Wang, D.W. Gross, K.E. Nygren, Hydrogen Embrittlement Understood, Metallurgical and Materials Transactions A 46 (2015) 2323–2341. https://doi.org/10.1007/s11661-015-2836-1.

[10] S. Lynch, Hydrogen embrittlement phenomena and mechanisms, Corrosion Reviews 30 (2012) 105–123. https://doi.org/10.1515/corrrev-2012-0502.

[11] R.A. Oriani, The diffusion and trapping of hydrogen in steel, Acta Metallurgica 18 (1970) 147–157. https://doi.org/10.1016/0001-6160(70)90078-7.

[12] M.A. Kappes, T.E. Perez, Blending hydrogen in existing natural gas pipelines: Integrity consequences from a fitness for service perspective, Journal of Pipeline Science and Engineering 3 (2023). https://doi.org/10.1016/j.jpse.2023.100141.

[13] J. Wijnen, J. Parker, M. Gagliano, E. Martínez-Pañeda, Virtual failure assessment diagrams for hydrogen transmission pipelines, Int. J. Hydrogen Energy 149 (2025). https://doi.org/10.1016/j.ijhydene.2025.06.174.

[14] V. Hasanli, Quantifying conservatism in ASME B31.12 Option A for hydrogen pipeline repurposing, Int. J. Hydrogen Energy 191 (2025). https://doi.org/10.1016/j.ijhydene.2025.152188.

[15] M. Sánchez, N. Marinova, E. Silveira, N. Larrosa, Standards and codes for hydrogen in pipeline infrastructure: testing, qualification, and integrity assessment, Journal of Pipeline Science and Engineering 5 (2025). https://doi.org/10.1016/j.jpse.2025.100296.

[16] Deutscher Verein des Gas- und Wasserfaches, DVGW G 464 (M): Fracture-Mechanical Assessment Concept for Steel Pipelines with a Design Pressure of more than 16 bar for the Transport of Hydrogen, (n.d.).

The research leading to these results has received funding from Horizon Europe, the European Union's Framework Programme for Research and Innovation under grant agreement n° 101111888.

[17] DIN EN 1594/A1:2025-08 - Draft Gas infrastructure - Pipelines for maximum operating pressure over 16 bar - Functional requirements; German and English version EN 1594:2024/prA1:2025, (2025). https://doi.org/10.31030/3629197.

[18] C. San Marchi, J.A. Ronevich, P. Bortot, M. Ortolani, K. Xu, M. Rana, Technical Basis for Fatigue Crack Growth Rules in Gaseous Hydrogen for ASME B31.12 Code Case 220 and for Revision of ASME VIII-3 Code Case 2938-1, in: Volume 4: Materials & Fabrication, American Society of Mechanical Engineers, 2024. https://doi.org/10.1115/PVP2024-122529.

[19] ASTM, ASTM E1049 Standard Practices for Cycle Counting in Fatigue Analysis, (2023).

[20] D. Stalheim, T. Boggess, D. Bromley, S. Jansto, S. Ningileri, Continued Microstructure and Mechanical Property Performance Evaluation of Commercial Grade API Pipeline Steels in High Pressure Gaseous Hydrogen, in: Volume 3: Materials and Joining, American Society of Mechanical Engineers, 2012: pp. 275–283. https://doi.org/10.1115/IPC2012-90313.

[21] H.P. Kyriakopoulou, I.D. Belntekos, A.S. Tazedakis, N.M. Daniolos, P. Karmiris-Obratański, D.I. Pantelis, Investigation of the Correlation between Hydrogen Cathodic Charging Conditions and Toughness Properties of Longitudinal Submerged Arc Welded X65 Pipeline Steels, J. Mater. Eng. Perform. 29 (2020) 3205–3219. https://doi.org/10.1007/s11665-020-04864-0.

[22] T.T. Nguyen, H.M. Heo, J. Park, S.H. Nahm, U.B. Beak, Fracture properties and fatigue life assessment of API X70 pipeline steel under the effect of an environment containing hydrogen, Journal of Mechanical Science and Technology 35 (2021) 1445–1455. https://doi.org/10.1007/s12206-021-0310-0.

[23] H. Wei, H. Tang, B. Xing, J. Shang, S. Qiu, Z. Hua, C. Gu, Research on the fracture toughness of pipeline steel X80 in a hydrogen environment, Eng. Fail. Anal. 180 (2025). https://doi.org/10.1016/j.engfailanal.2025.109917.

[24] Y. Yang, L. Shi, Z. Xu, H. Lu, X. Chen, X. Wang, Fracture toughness of the materials in welded joint of X80 pipeline steel, Eng. Fract. Mech. 148 (2015) 337–349. https://doi.org/10.1016/j.engfracmech.2015.07.061.

[25] E. V. Chatzidouros, V.J. Papazoglou, T.E. Tsiourva, D.I. Pantelis, Hydrogen effect on fracture toughness of pipeline steel welds, with in situ hydrogen charging, Int. J. Hydrogen Energy 36 (2011) 12626–12643. https://doi.org/10.1016/j.ijhydene.2011.06.140.

[26] E. V. Chatzidouros, V.J. Papazoglou, D.I. Pantelis, Hydrogen effect on a low carbon ferritic-bainitic pipeline steel, Int. J. Hydrogen Energy 39 (2014) 18498–18505. https://doi.org/10.1016/j.ijhydene.2014.09.029.

[27] S. Huang, H. Hui, Predictive environmental hydrogen embrittlement on fracture toughness of commercial ferritic steels with hydrogen-modified fracture strain model, Int. J. Hydrogen Energy 47 (2022) 10777–10787. https://doi.org/10.1016/j.ijhydene.2021.12.128.

[28] H. Wei, B. Duan, X. Shi, R. Gao, Z. Hua, S. Qiu, Y. Zhao, Influence of hydrogen in natural gas mixed hydrogen environment on mechanical properties of X80 pipeline steel, Int. J. Hydrogen Energy 54 (2024) 908–921. https://doi.org/10.1016/j.ijhydene.2023.09.138.

[29] M.L. Martin, M. Connolly, Z.N. Buck, P.E. Bradley, D. Lauria, A.J. Slifka, Evaluating a natural gas pipeline steel for blended hydrogen service, J. Nat. Gas Sci. Eng. 101 (2022). https://doi.org/10.1016/j.jngse.2022.104529.

[30] J. Shang, J.Z. Wang, W.F. Chen, H.T. Wei, J.Y. Zheng, Z.L. Hua, L. Zhang, C.H. Gu, Different effects of pure hydrogen vs. hydrogen/natural gas mixture on fracture toughness degradation of two carbon steels, Mater. Lett. 296 (2021). https://doi.org/10.1016/j.matlet.2021.129924.

The research leading to these results has received funding from Horizon Europe, the European Union's Framework Programme for Research and Innovation under grant agreement n° 101111888.

[31] D. Hejazi, A.J. Haq, N. Yazdipour, D.P. Dunne, A. Calka, F. Barbaro, E. V. Pereloma, Effect of manganese content and microstructure on the susceptibility of X70 pipeline steel to hydrogen cracking, Materials Science and Engineering: A 551 (2012) 40–49. https://doi.org/10.1016/j.msea.2012.04.076.

[32] M.P. Singh, K.S. Arora, R. Kumar, D.K. Shukla, S. Siva Prasad, Influence of heat input on microstructure and fracture toughness property in different zones of X80 pipeline steel weldments, Fatigue Fract. Eng. Mater. Struct. 44 (2021) 85–100. https://doi.org/10.1111/ffe.13333.

[33] D. Stalheim, T. Boggess, C. San Marchi, S. Jansto, B. Somerday, G. Muralidharan, P. Sofronis, Microstructure and Mechanical Property Performance of Commercial Grade API Pipeline Steels in High Pressure Gaseous Hydrogen, in: 2010 8th International Pipeline Conference, Volume 2, ASMEDC, 2010: pp. 529–537. https://doi.org/10.1115/IPC2010-31301.

[34] E. V. Chatzidouros, V.J. Papazoglou, D.I. Pantelis, Hydrogen Effect on Fracture Toughness of API 5L X70, X65 and X52 Pipeline Steel Welds: An Overview, in: Volume 3: Materials Technology; Jan Vugts Symposium on Design Methodology of Offshore Structures; Jo Pinkster Symposium on Second Order Wave Drift Forces on Floating Structures; Johan Wichers Symposium on Mooring of Floating Structures in Waves, ASMEDC, 2011: pp. 251–260. https://doi.org/10.1115/OMAE2011-49348.

[35] B.P. Somerday, C.S. Marchi, K.A. Nibur, D.G. Stalheim, T. Boggess, S. Jansto, Fracture and fatigue of commercial grade API pipeline steels in gaseous hydrogen, 2011.

[36] K. Xu, Hydrogen embrittlement of carbon steels and their welds, in: R.P. Gangloff, B.P. Somerday (Eds.), Gaseous Hydrogen Embrittlement of Materials in Energy Technologies, Elsevier, 2012: pp. 526–561. https://doi.org/10.1533/9780857093899.3.526.

[37] H.P. Kyriakopoulou, P. Karmiris-Obratański, A.S. Tazedakis, N.M. Daniolos, E.C. Dourdounis, D.E. Manolakos, D. Pantelis, Investigation of hydrogen embrittlement susceptibility and fracture toughness drop after in situ hydrogen cathodic charging for an X65 pipeline steel, Micromachines (Basel). 11 (2020). https://doi.org/10.3390/MI11040430.

[38] M. Steiner, U. Marewski, H. Silcher, DVGW Project SyWeSt H2: "Investigation of Steel Materials for Gas Pipelines and Plants for Assessment of their Suitability with Hydrogen" Final Report, 2023.

[39] W.R. Hoover, S.L. Robinson, R.E. Stoltz, J.R. Spingarn, Hydrogen compatibility of structural materials for energy storage and transmission, NASA STI/Recon Technical Report N 81 (1981) 29598.

[40] S. Wen, H. Dong, S.Y. Zhang, A. Bannister, M. Connelly, Neutron diffraction measurement of weld residual stresses in an UOE linepipe subjected to mechanical expansion, in: OMAE 2013, 2013: p. 11257.

[41] B. Meng, C. Gu, L. Zhang, C. Zhou, X. Li, Y. Zhao, J. Zheng, X. Chen, Y. Han, Hydrogen effects on X80 pipeline steel in high-pressure natural gas/hydrogen mixtures, Int. J. Hydrogen Energy 42 (2017) 7404–7412. https://doi.org/10.1016/j.ijhydene.2016.05.145.

[42] Erik Smedberg, Aurelien Pitois, Rémi Kleine, Beatriz Acosta Iborra, Pipelines for hydrogen transport: A review of integrity and safety challenges, 2025. https://doi.org/10.2760/4545832.

[43] E.W. Collings, H.J. Cialone, E.J. Drauglis, HYDROGEN DEGRADATION OF PIPELINE STEELS FINAL REPORT, 1986.

[44] V. Srikrishnan, P.J. Ficalora, Selective Adsorption and Hydrogen Embrittlement, METALLURGICAL TRANSACTIONS A (1976).

[45] M. Röthig, J. Hoschke, C. Tapia, J. Venezuela, A. Atrens, A review of gas phase inhibition of gaseous hydrogen embrittlement in pipeline steels, Int. J. Hydrogen Energy 60 (2024) 1239–1265. https://doi.org/10.1016/j.ijhydene.2024.02.245.

[46] Y. Sun, Y. Ren, Y.F. Cheng, Dissociative adsorption of hydrogen and methane molecules at high-angle grain boundaries of pipeline steel studied by density functional theory modeling, Int. J. Hydrogen Energy 47 (2022) 41069–41086. https://doi.org/10.1016/j.ijhydene.2022.09.173.

The research leading to these results has received funding from Horizon Europe, the European Union's Framework Programme for Research and Innovation under grant agreement n° 101111888.

[47] C. Liu, H. Yang, C. Wang, H. Zhang, R. Ding, L. Ai, X. Fan, R. Zhang, X. Xu, Y. Ning, Y.F. Cheng, Y. Li, Effects of CH4 and CO on hydrogen embrittlement susceptibility of X80 pipeline steel in hydrogen blended natural gas, Int. J. Hydrogen Energy 48 (2023) 27766–27777. https://doi.org/10.1016/j.ijhydene.2023.03.443.

[48] J. Shang, R. Gao, B. Xing, H. Wei, Z. Hua, Enhanced hydrogen degradation of two pipeline steels by increasing inert gas pressure in hydrogen-containing mixtures: experimental and theoretical insights, Corros. Sci. 240 (2024). https://doi.org/10.1016/j.corsci.2024.112466.

[49] J. Shang, Z. Hua, B. Xing, H. Wei, J. Zheng, Enhanced hydrogen embrittlement of steel by the premature hydrogen dissociation with the increasing inert gas pressure in hydrogen-containing mixtures, Acta Mater. 259 (2023). https://doi.org/10.1016/j.actamat.2023.119279.

[50] Holbrook JH, . Cialone HJ, Hydrogen degradation of pipeline steels. Summary report, 1984.

[51] R. Zhang, C. Yuan, C. Liu, C. Wang, X. Xu, J. Zhang, Y. Li, Effects of natural gas impurities on hydrogen embrittlement susceptibility and hydrogen permeation of X52 pipeline steel, Eng. Fail. Anal. 159 (2024). https://doi.org/10.1016/j.engfailanal.2024.108111.

[52] C. Zhou, H. Zhou, L. Zhang, The Impact of Impurity Gases on the Hydrogen Embrittlement Behavior of Pipeline Steel in High-Pressure H2 Environments, Materials 17 (2024). https://doi.org/10.3390/ma17092157.

[53] J. Shang, W. Chen, J. Zheng, Z. Hua, L. Zhang, C. Zhou, C. Gu, Enhanced hydrogen embrittlement of low-carbon steel to natural gas/hydrogen mixtures, Scr. Mater. 189 (2020) 67–71. https://doi.org/10.1016/j.scriptamat.2020.08.011.

[54] D. Cui, Y. Bai, L. Xiong, B. Yu, B. Wei, C. Sun, Effects of hydrogen blending ratios and CO2 on hydrogen embrittlement of X65 steel in high-pressure offshore hydrogen-blended natural gas pipelines, Journal of Materials Research and Technology 33 (2024) 4763–4771. https://doi.org/10.1016/j.jmrt.2024.10.150.

[55] J. Shang, J. Guo, B. Xing, R. Gao, Z. Hua, CO2 effect on the fatigue crack growth of X80 pipeline steel in hydrogen-enriched natural gas: Experiment vs DFT, Int. J. Hydrogen Energy 66 (2024) 636–644. https://doi.org/10.1016/j.ijhydene.2024.04.116.

[56] J. Shang, S. Chi, R. Gao, B. Xing, A. Staykov, Z. Hua, Pressure dependence of CO2 effect on hydrogen-assisted fatigue crack growth in two pipeline steels, Int. J. Hydrogen Energy 90 (2024) 842–852. https://doi.org/10.1016/j.ijhydene.2024.10.032.

[57] C. Zhou, H. Wu, H. Chen, X. Yan, Y. Qian, K. Zhang, L. Zhang, J. Shang, The influence of CO2 partial pressure on the hydrogen embrittlement behavior of pure iron in high-pressure hydrogen environment, Corros. Sci. 260 (2026). https://doi.org/10.1016/j.corsci.2025.113555.

[58] S. Rhythm, R. Ahmed, N. Ahmed, M. Gyaabeng, C. Teodoriu, Experimental study of the impact of hydrogen embrittlement on the ductility of natural gas pipeline steels, Gas Science and Engineering 143 (2025). https://doi.org/10.1016/j.jgsce.2025.205746.

[59] R.P. Gangloff, B.P. Somerday, Gaseous hydrogen embrittlement of materials in energy technologies Volume 2, 2012. https://doi.org/10.1533/9780857095374.

[60] J. Zhou, M. Wu, J. Qiu, R. Cheng, M. Tian, Influence of H2S on the Hydrogen Embrittlement Susceptibility of X80 Pipeline Steel in Hydrogen-Doped Natural Gas, ACS Omega 10 (2025) 28233–28242. https://doi.org/10.1021/acsomega.5c03111.

[61] A. Islam, T. Alam, N. Sheibley, K. Edmonson, D. Burns, M. Hernandez, Hydrogen blending in natural gas pipelines: A comprehensive review of material compatibility and safety considerations, Int. J. Hydrogen Energy 93 (2024) 1429–1461. https://doi.org/10.1016/j.ijhydene.2024.10.384.

[62] D.R. Michanowicz, O.M. Leventhal, J.K. Domen, S.R. Williams, E.D. Lebel, L.A.L. Hill, J.J. Buonocore, C.L. Nordgaard, A.S. Bernstein, S.B.C. Shonkoff, Natural gas odorants: A scoping review

of health effects, Curr. Environ. Health Rep. 10 (2023) 337–352. https://doi.org/10.1007/s40572-023-00403-w.

[63] MARCOGAZ, NATURAL GAS ODORISATION PRACTICES IN EUROPE ABOUT MARCOGAZ, 2023. www.marcogaz.org.

[64] S. Fukuyama, K. Yokogawa, M. Araki, Fracture toughness and fatigue crack growth of AISI 4340 steel in high pressure hydrogen at room temperature., Design & Analysis (1989) 1181–1188. https://doi.org/10.1016/B978-1-4832-8430-9.50116-7.

[65] S. Bartlett, J. Hesketh, H. Becker, G. Hinds, Project closure report Hydrogen Odorant and Leak Detection Part 1, Hydrogen Odorant, 2020.

[66] ONTZHi Project , Https://Www.Ontzhi.Com/En (n.d.).

[67] A. Hamed, M. Beschliesser, S. Fink, G. Mori, The effect of hydrogen odorisation with mercaptans on hydrogen uptake in L360NB pipeline steel: An experimental study, Fuel 418 (2026) 138812. https://doi.org/10.1016/j.fuel.2026.138812.

[68] Open Grid Europe , (n.d.). https://oge.net/_Resources/Persistent/1/8/b/e/18be93c08cf94cda2e88f49b29988e2e2e96cc67/Orientierungswerte%202024_Stand11_03_2025.pdf (accessed July 23, 2026).

[69] MARCOGAZ, Liquefied Natural Gas (LNG) quality database Gas composition and main properties, 2024. https://www.marcogaz.org/publications/liquefied-natural-gas-lng-quality-database/ (accessed May 20, 2026).

[70] European Standard, EN 16726 Gas infrastructure- Quality of gas-Group H, (n.d.).

[71] CSA ANSI/CSA CHMC 1-2014 (R2018) - Test methods for evaluating material compatibility in compressedhydrogen applications - Metals, (n.d.). https://webstore.ansi.org/standards/csa/csaansichmc2014r2018 (accessed May 3, 2022).

[72] ASTM, ASTM G129Standard Practice for Slow Strain Rate Testing to Evaluate the Susceptibility of Metallic Materials to Environmentally Assisted Cracking 1, 2006. https://doi.org/10.1520/G0129-00R06.2.

[73] G142-98(2004), Standard Test Method for Determination of Susceptibility of Metals to Embrittlement in Hydrogen Containing Environments at High Pressure , High Temperature, or Both, ASTM Book of Standards 03 (1998) 1–8. https://doi.org/10.1520/G0142-98R16.2.

[74] H. Wei, B. Duan, X. Shi, R. Gao, Z. Hua, S. Qiu, Y. Zhao, Influence of hydrogen in natural gas mixed hydrogen environment on mechanical properties of X80 pipeline steel, Int. J. Hydrogen Energy 54 (2024) 908–921. https://doi.org/10.1016/j.ijhydene.2023.09.138.

Shimmer

The research leading to these results has received funding from Horizon Europe, the European Union's Framework Programme for Research and Innovation under grant agreement n° 101111888.